Mon. Not. R. Astron. Soc. **363,** 479–495 (2005) doi:10.1111/j.1365-2966.2005.09432.x

A homogeneous sample of sub-damped Lyman α systems – III. Total gas mass $\Omega_{\rm H\,I+He\,II}$ at $z > 2^{\star}$

Céline Péroux,[1]† Miroslava Dessauges-Zavadsky,[2] Sandro D'Odorico,[1] Tae Sun Kim[3] and Richard G. McMahon[3]

[1]*European Southern Observatory, Karl-Schwarzchild-Strasse 2, 85748 Garching-bei-München, Germany*
[2]*Observatoire de Genève, 1290 Sauverny, Switzerland*
[3]*Institute of Astronomy, Madingley Road, Cambridge CB3 0HA*

Accepted 2005 July 13. Received 2005 July 13; in original form 2005 February 1

ABSTRACT

Absorbers seen in the spectrum of background quasars are a unique tool with which to select H I-rich galaxies at all redshifts. In turns, these galaxies allow us to determine the cosmological evolution of the H I gas $\Omega_{\rm H\,I+He\,II}$, which is a possible indicator of gas consumption as star formation proceeds. The damped Lyman α (Lyα) systems (DLAs with $N_{\rm H\,I} \geqslant 10^{20.3}\,{\rm cm}^{-2}$), in particular, are believed to contain a large fraction of the H I gas but there are also indications that lower column-density systems, called 'sub-damped Lyα' systems, play a role at high redshift. Here we present the discovery of high-redshift sub-DLAs based on 17 $z > 4$ quasar spectra observed with the Ultraviolet–Visual Echelle Spectrograph (UVES) on the Very Large Telescope (VLT). This sample is composed of 21 new sub-DLAs which, together with another 10 systems from previous European Southern Observatory archive studies, make up a homogeneous sample. The redshift evolution of the number density of several classes of absorbers is derived and shows that all systems seem to be evolving in the redshift range from $z = 5$ to $z \sim 3$. These results are further used to estimate the redshift evolution of the characteristic radius of these classes of absorbers, assuming a Holmberg relation and one unique underlying parent population. DLAs are found to have $R_* \sim 20\,h_{100}^{-1}$ kpc, while sub-DLAs have $R_* \sim 40\,h_{100}^{-1}$ kpc. The redshift evolution of the column density distribution, f(N,z), down to $N_{\rm H\,I} = 10^{19}\,{\rm cm}^{-2}$ is also presented. A departure from a power law due to a flattening of f(N,z) in the sub-DLA regime is present in the data. f(N,z) is further used to determine the H I gas mass contained in sub-DLAs at z > 2. The complete sample shows that sub-DLAs are important at all redshifts from $z = 5$ to $z = 2$. Finally, the possibility that sub-DLAs are less affected by the effects of dust obscuration than classical DLAs is discussed.

Key words: galaxies: abundances – galaxies: high-redshift – quasars: absorption lines – quasars: general.

1 INTRODUCTION

Tracing the rate at which stars form over cosmological scales still remains a challenging observational task. An indirect way to probe the assembly of galaxies is to probe the rate at which they convert their gas into stars. The neutral H I mass in particular can be estimated from observations of absorbers seen in the spectrum of background quasars. Unlike other high-redshift galaxies (such as Lyman Break Galaxies, Steidel et al. 2003), these objects are selected solely on their H I cross-sections regardless of their intrinsic luminosities or star formation rates. The quasar absorption systems are divided into several classes according to the number of atoms along the observed line of sight: the Lyman α (Lyα) forest have H I column densities ranging from $\simeq 10^{12}$ to $1.6 \times 10^{17}\,{\rm atom\,cm}^{-2}$, the Lyman-limit systems (LLSs) with $N({\rm H\,I}) > 1.6 \times 10^{17}\,{\rm atom\,cm}^{-2}$ and the damped Lyα systems (DLAs) with $N({\rm H\,I}) > 2 \times 10^{20}\,{\rm atom\,cm}^{-2}$. These latter systems are believed to be the major contributors to the neutral gas in the Universe at high redshifts. They thus can be used to measure the redshift evolution of $\Omega_{\rm H\,I+He\,II}$, the total amount of neutral gas expressed as a fraction of today's critical density (Lanzetta et al.

⋆Based on observations collected during programme ESO 69.A-0613, ESO 71.A-0114 and ESO 73.A-0653 at the European Southern Observatory with the Ultraviolet-Visual Echelle Spectrograph on the 8.2 m Kueyen telescope operated at the Paranal Observatory, Chile.

†E-mail: cperoux@eso.org

1991; Wolfe et al. 1995; Storrie-Lombardi, Irwin & McMahon 1996a; Storrie-Lombardi & Wolfe 2000). We have recently suggested (Péroux et al. 2003a) that at $z > 3.5$, some fraction of the H I lies in systems below the traditional DLA definition, in 'sub-damped Lyα systems (sub-DLAs)' with $19 < \log N(\mathrm{H\,I}) < 20.3$ cm^{-2}. The name arises from the fact that this column-density range lies on the linear part of the curve of growth which links the equivalent width of an absorber to the number of atoms along the line of sight. The present paper reviews these predictions based on direct observations of a sample of sub-DLAs.

In addition, quasar absorbers are direct indicators of element abundances over >90 per cent of the age of the Universe. The cosmological evolution of the H I column-density weighted metallicity (e.g. Kulkarni & Fall 2002) shows surprising results: contrary to virtually all chemical models (e.g. Malaney & Chaboyer 1996; Pei, Fall & Hauser 1999), the most recent observations indicate mild evolution with redshift (Khare et al. 2004; Kulkarni et al. 2005). Therefore, the results to date might give a biased or incomplete view of the global galactic chemical evolution. The ultimate goal of this project is to undertake detailed abundance and dynamical studies of an appropriate sample of sub-DLAs in order to estimate the evolution of their mean abundance with redshift.

In a first step towards this goal, we took advantage of the European Southern Observatory's (ESO) Very Large Telescope (VLT) archive to build a sample of sub-DLAs by analysing Ultraviolet-Visual Echelle Spectrograph (UVES) archival echelle QSO spectra. This represents a sample of 35 QSOs, 22 of which were unbiased for our study. This study led to the discovery of 12 sub-DLAs (Dessauges-Zavadsky et al. 2003). Their chemical abundances were derived using Voigt profile fitting and photoionization models from the CLOUDY software package in order to determine the ionization correction. We find that the correction is negligible in systems with $N(\mathrm{H\,I}) > 3.2 \times 10^{19}$ and lower than 0.3 dex for most elements in systems with $10^{19} < N(\mathrm{H\,I}) < 3.2 \times 10^{19}$ atom cm^{-2}. These systems were used to observationally determine the shape of the column density distribution, $f(N, z)$, down to $N(\mathrm{H\,I}) = 10^{19}$ cm^{-2} (Péroux et al. 2003b), although the lack of high-redshift systems prevented us from measuring the $f(N, z)$ redshift evolution. The abundances observed in this sample of sub-DLAs were further used to determine the global metallicity of H I gas in both DLAs and sub-DLAs.

Here we present a new sample of 17 $z > 4$ quasar lines of sight observed at high resolution with UVES on the VLT. We use these newly acquired data to search for and study the statistical properties of high-redshift sub-DLAs. In Section 2 the observations and the data reduction process are given in detail, together with a description of each object. Section 3 presents the statistical characteristics of the survey and the newly built sub-DLA sample. Finally, our

Table 1. Journal of observations of our observing programmes to find and analyse new high-redshift sub-DLAs in 17 $z > 4$ quasars.

Quasar	Alternative name	z_{em}	R mag	Obs Date	UVES settings	Exp. Time (s)	Ref
BR J0006−6208	...	4.455	19.25	27 Sept 2002	580	7200	1
PSS J0118 + 0320$^{\mathrm{red}}$	...	4.230	18.66	2002 Sept 28	560	3600	6
...	...	...	...	2003 Sept 01	390+580	5400	...
...	...	...	...	2003 Sept 01	580	5400	...
...	...	...	...	2003 Sept 01	860	5400×2	...
PSS J0121 + 0347$^{\mathrm{red*}}$	...	4.127	18.33	2002 Sept 28	540	3600	5
...	...	...	...	2003 Sept 02	470+800	3600×2	...
SDSS J0124 + 0044$^{\mathrm{red}}$	...	3.840	17.75	2002 Sept 27	520	3600	4
...	...	...	...	2003 Sept 02	520	3600	...
...	...	...	...	2004 Aug 29/Sept 04	580	3000×4	...
PSS J0133+0400	...	4.154	18.32	2002 Sept 27	520	3600	1,7
BRI J0137 − 4224$^{\mathrm{red}}$	BRI B0135−4239	3.970	18.77	2002 Sept 27	520	3600	3
...	...	...	...	2003 Sept 03	520	5000	...
...	...	...	...	2003 Sept 03	470+800	3600+4500	...
PSS J0209+0517	...	4.174	17.76	2002 Sept 28	390+580	7200	1,7
BRI J0244−0134	BRI B0241−0146	4.053	18.18	2002 Sept 27	520	3600	2
BR J0311−1722	...	4.039	17.73	2002 Sept 28	540	3600	1
BR J0334 − 1612$^{\mathrm{red}}$	...	4.363	17.86	2002 Sept 28	560	3600	1
...	...	...	...	2003 Sept 02	580	3600×2	...
...	...	...	...	2003 Sept 02	860	5066	...
BR J0419−5716	...	4.461	17.78	2002 Sept 28	560	1846	1
BR J2017 − 4019$^{\mathrm{BAL}}$	BRLCO B2013−4028	4.131	18.60	2003 Sept 03	540	3600	1
PSS J2154+0335	...	4.363	19.05	2002 Sept 28	560	3600	1
BR J2215 − 1611$^{\mathrm{red}}$	BR B2212−1626	3.990	18.10	2002 Sept 28	540	3600	2
...	...	...	...	2003 Sept 03	540	3600+1215	...
...	...	...	...	2003 Sept 03	470+800	3600×2	...
BR J2216 − 6714$^{\mathrm{red}}$	...	4.469	18.57	2002 Sept 28	560	3600	1
...	...	...	...	2003 Sept 01	560	3600×2	...
...	...	...	...	2003 Sept 01	580	5400	...
...	...	...	...	2003 Sept 02	860	5400×2	...
BR J2239−0552	BR B2237−0607	4.558	18.30	2002 Sept 27	580	3600	2
BR J2349−3712	BRLCO B2346−3729	4.208	18.70	2003 Sept 03	540	3600	1

$^{\mathrm{BAL}}$:affected by broad absorption line features. $^{\mathrm{red}}$:spectrum with complete wavelength coverage including the red of the Ly-α emission line. $^{\mathrm{red*}}$:attempt to get a spectrum with complete wavelength coverage impaired by bad weather conditions (strong northern wind).
References: (1) Péroux et al. (2001); (2) Storrie-Lombardi et al. (1996a); (3) Storrie-Lombardi et al. (2001); (4) Schneider et al. 2002; (5) Stern et al. 2000; (6) from the Palomar Sky Survey, see http://www.astro.caltech.edu/∼george/z4.qsos; (7) Prochaska et al. (2003).

current state of knowledge of this class of absorbers together with implications for the cosmological evolution of H I gas mass are discussed in Section 4.

2 THE $Z > 2$ SUB-DLA SAMPLE

2.1 Observations and data reduction

In order to complement the previous study and analyse sub-DLAs at $z > 3$, we started in 2002 September to build a UVES sample of high-redshift QSOs never observed before at high resolution. This snapshot is carefully designed to determine the redshift evolution of the statistical properties of sub-DLAs (number density and column density distribution). The second step of the observing programme, undertaken a year later in 2003 September, aims at concentrating on the seven most promising targets that would enable detailed metallicity and dynamical studies at high redshifts. An extra set of data was obtained on 2004 August 29, 2004 September 2 and 4, in service mode in the framework of a parallel observing programme (ESO 73.A-0653; principal investigator N. Bouché). Table 1 gives the journal of the observations.

The data reduction of the observations from periods 69 and 71 is done using the version of the UVES pipeline within the MIDAS environment available at the time (version: UVES/2.0.0 FLMIDAS/1.0.0). The newest data (period 73) are reduced with the most recent version of the pipeline to accommodate the new format of the raw fits file (version: UVES/2.1.0 FLMIDAS/1.1.0). The raw wavelength frames are inspected closely to optimize the number of echelle orders to be extracted for each CCD. Master bias and flat images are constructed using calibration frames taken nearest in time to the science frames. Lamp images are taken on various occasions throughout the observing nights to be able to make accurate wavelength calibrations. In most cases, the science frames and associated stars are extracted with the 'optimal' option. Nevertheless, on a few frames from the second observing run (2003 September), two of the settings (540 and 800) show a periodic feature of the order of a few Angströms. These features are not present when these few frames are extracted using the 'average' option followed by a cosmic filtering.

For the seven objects that were observed with more than one setting, the resulting spectra are combined by using the signal-to-noise ratio (S/N) of the spectrum as a weight. The final spectra have a resolution of 7 km s^{-1}. In some cases, we notice that the parts of the spectra that are fully absorbed do not actually reach the zero flux level. This problem is known to occur when there are not enough photons in the sky area. Indeed, the optimal extraction is done to fit a Gaussian profile and the baseline of the Gaussian is the sky level. If the seeing during the observations is poor and the exposure short, it is possible that at blue wavelengths, only a few photons fall on the sky pixel. This leads to high photon-noise and might produce the under-subtraction of the sky level. The unsaturated absorption lines are unaffected by this zero-level problem. In the case of saturated

Table 2. High-redshift quasar absorber sample composed of 21 sub-DLAs and seven DLAs.

Quasar	$z_{\rm em}$	$z_{\rm abs}$	log $N_{\rm H\,I}$	Ly series	metals	Note
BR J0006−6208	4.455	3.202	20.80±0.10	Ly1	no metals over available coverage	DLA
...	...	4.145	19.37±0.15	Ly3	no metals over available coverage	...
PSS J0118 + 0320$^{\rm red}$	4.230	4.128	20.02±0.15	Ly5	Fe II, Si II, O I, C II, Si IV, C IV	...
PSS J0121 + 0347$^{\rm red*}$	4.127	2.976	19.53±0.10	Ly1	O I, C IV, Fe II, Al II	...
SDSS J0124 + 0044$^{\rm red}$	3.840	2.988	19.18±0.10	Ly1	Si II, C IV, Fe II, Al II	...
...	...	3.078	20.21±0.10	Ly1	C II, Si II, O I, Si IV, C IV, Fe II	...
PSS J0133+0400	4.154	3.139	19.01±0.10	Ly1	Ni II, C II	...
...	...	3.692	20.68±0.15	Ly2	no metals over available coverage	DLA
...	...	3.773	20.42±0.10	Ly2	no metals over available coverage	DLA
...	...	3.995	19.94±0.15	Ly4	no metals over available coverage	blended with the following system
...	...	3.999	19.16±0.15	Ly4	no metals over available coverage	blended with the previous system
...	...	4.021	19.09±0.15	Ly4	Fe II	...
BRI J0137 − 4224$^{\rm red}$	3.970	3.101	19.81±0.10	Ly4	Si II, C IV, Fe II, Al II	...
...	...	3.665	19.11±0.10	Ly11	Si II, O I, C II, Si IV	...
PSS J0209+0517	4.174	3.666	20.47±0.10	Ly2	Si IV	DLA
...	...	3.707	19.24±0.10	Ly2	O I, Si IV	...
...	...	3.863	20.43±0.15	Ly3	Si II, O I, C II	DLA
BRI J0244−0134	4.053	...	...	...	...	...
BR J0311−1722	4.039	3.734	19.48±0.10	Ly7	Si II, O I, C II	...
BR J0334 − 1612$^{\rm red}$	4.363	3.557	21.12±0.15	Ly1	Si II, C IV, Fe II, Al II, Zn II	DLA
BR J0419−5716	4.461	3.063	19.17±0.10	Ly1	O I	...
BR J2017 − 4019$^{\rm BAL}$	4.131	...	...	...	...	...
PSS J2154+0335	4.363	3.177	19.23±0.15	Ly1	no metals over available coverage	...
BR J2215 − 1611$^{\rm red}$	3.990	3.656	19.01±0.15	Ly3	Ni II, C II, Zn II	blended with the following system
...	...	3.662	20.05±0.15	Ly3	O I, C II, Si IV, Si II, C IV, Fe II, Al II	blended with the previous system
BR J2216 − 6714$^{\rm red}$	4.469	3.368	19.80±0.10	Ly1	C II, C IV, Al II	...
BR J2239−0552	4.558	4.079	20.55±0.10	Ly3	Si II, O I, C II	DLA
BR J2349−3712	4.208	3.581	19.12±0.10	Ly2	no metals over available coverage	...
...	...	3.690	19.79±0.15	Ly2	no metals over available coverage	blended with the following system
...	...	3.696	19.78±0.10	Ly2	no metals over available coverage	blended with the previous system

$^{\rm BAL}$:affected by broad absorption line features. $^{\rm red}$:spectrum with complete wavelength coverage including to the red of the Lyα emission line. $^{\rm red*}$:attempt to get a spectrum with complete wavelength coverage impaired by bad weather conditions (strong northern wind).

lines, we correct the spectrum by subtracting a few per cent from the continuum level value. The spectra are then normalized using a spline function to join the part of the continuum that is free of absorption lines.

2.2 Identification and column density measurements of absorbers

The method of searching for sub-DLAs in the spectra described above very much follows the method used in our previous studies (Dessauges-Zavadsky et al. 2003). We first use an automated detection algorithm supplemented further by visual searches independently undertaken by three of us (CP, MD-Z and T-SK). Although the forest of the quasars at these redshifts is considerably absorbed by foreground structures, the presence of damping wings down to the Ly2, and occasionally to higher lines of the series, provides an unambiguous signature of damped absorbers. We also report the detection of metal lines at the associated redshifts, although this is not used as a criterion for sub-DLA selection. Table 2 summarizes this information together with the redshifts, H I column densities and the references of the seven DLAs and 21 sub-DLAs found in our new high-redshift quasar sample. The latter systems span a range of H I column densities from $10^{19.01}$ to $10^{20.21}$ cm^{-2} with $z_{\rm abs} = 2.976$ to 4.145.

The H I column-density measurements are determined by fitting a Voigt profile to the absorption line. The fits were performed using the χ^2 minimization routine FITLYMAN in MIDAS (Fontana & Ballester 1995). The Doppler parameter b-value was usually fixed at 20 km s^{-1} or left as a free parameter, since in that high column-density regime, the sub-DLA systems $N_{\rm H\,I}$ are independent of the b-value. The fit is performed using the higher members of the Lyman series where these are available. The typical resulting error bar in $\log N_{\rm H\,I}$ measurements is 0.10 and never exceeds 0.15, but does not include errors in the continuum placement which we expect would not exceed 10 per cent.

2.3 Notes on individual objects

In this section, we provide details on each of the identified absorbers. Whenever the spectral coverage is available, we search for metals associated with the Ly lines among the 20 transitions most frequently detected in high column-density quasar absorbers.

(i) BR J0006−6208 ($z_{\rm em} = 4.455$). Péroux et al. (2001) have reported four candidate absorbers at $z_{\rm abs} = 2.97$, 3.20, 3.78 and 4.14 in the medium-resolution spectrum of this quasar. The blue end of the spectrum presented here is of fairly poor quality and therefore the minimum redshift above which quasar absorbers are searched for is set to $z_{\rm min} = 3.083$, so the lowest DLA cannot be taken into consideration upon. We confirm the presence of the $z_{\rm abs} = 3.202$ system and measure $\log N_{\rm H\,I} = 20.80 \pm 0.10$ in agreement with medium-resolution estimates. The third system, $z_{\rm abs} = 3.78$, falls in the UVES setting gap. The last absorber is confirmed as a sub-DLA with $\log N_{\rm H\,I} = 19.37 \pm 0.15$. No associated metal lines are detected over the limited wavelength coverage of our spectrum. Fig. 1 shows the best Voigt profile-fitting solutions for these two systems.

(ii) PSS J0118+0320 ($z_{\rm em} = 4.230$). This quasar was discovered as part of the Palomar Sky Survey and to our knowledge, there are no medium-resolution spectra published. We discovered an unambiguous sub-DLA at $z_{\rm abs} = 4.128$ and measure $\log N_{\rm H\,I} = 20.02 \pm 0.15$ down to the Lyman 5. Several associated metals are also observed in the red part of the spectrum. Fig. 2 shows our best fit of the H I lines.

(iii) PSS J0121+0347 ($z_{\rm em} = 4.127$). No absorbers have been previously reported in this quasar, also from the Palomar Sky Survey. We report here for the first time a sub-DLA with $\log N_{\rm H\,I} = 19.53 \pm 0.10$ at $z_{\rm abs} = 2.976$. Metal lines at that redshift are also observed in the red part of the spectrum. Fig. 3 shows our best fit of the H I line.

(iv) SDSS J0124+0044 ($z_{\rm em} = 3.840$). One absorber has been previously reported in this quasar from the Sloan Digital Sky Survey (Bouché & Lowenthal 2004). We report here for the first time the column density of the two sub-DLAs with $\log N_{\rm H\,I} = 19.18 \pm 0.10$ at $z_{\rm abs} = 2.988$ and $\log N_{\rm H\,I} = 20.21 \pm 0.10$ at $z_{\rm abs} = 3.078$. Metal lines at these redshifts are also observed in the red part of the spectrum. Fig. 4 shows our best fit of the H I lines.

(v) PSS J0133+0400 ($z_{\rm em} = 4.154$). Péroux et al. (2001) report two DLAs in this quasar which were further confirmed by observations made by Prochaska et al. (2003) using the Echellette Spectrograph and Imager (ESI) on the Keck II telescope. Here, we measure $\log N_{\rm H\,I} = 20.68 \pm 0.15$ at $z_{\rm abs} = 3.692$ and $\log N_{\rm H\,I} = 20.42 \pm 0.10$ at $z_{\rm abs} = 3.773$ (Prochaska et al. measure $\log N_{\rm H\,I} = 20.70^{+0.10}_{-0.15}$ and $\log N_{\rm H\,I} = 20.55^{+0.10}_{-0.15}$ respectively). We also note that these two

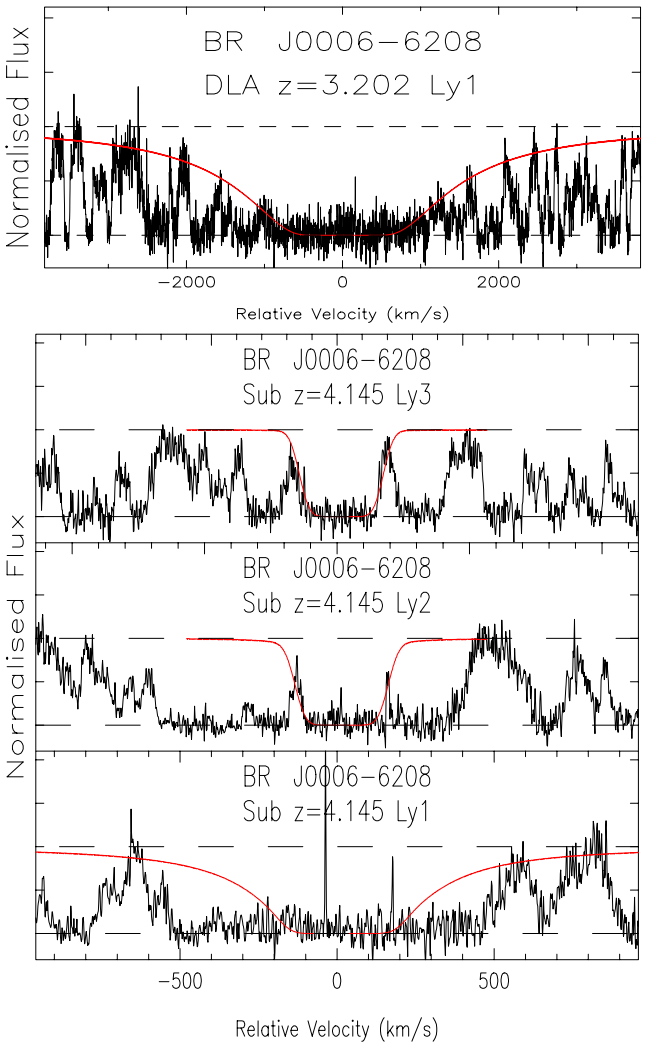

Figure 1. The two absorbers detected towards BR J0006−6208 at $z_{\rm abs} = 3.202$ ($\log N_{\rm H\,I} = 20.80 \pm 0.10$) and $z_{\rm abs} = 4.145$ ($\log N_{\rm H\,I} = 19.37 \pm 0.15$).

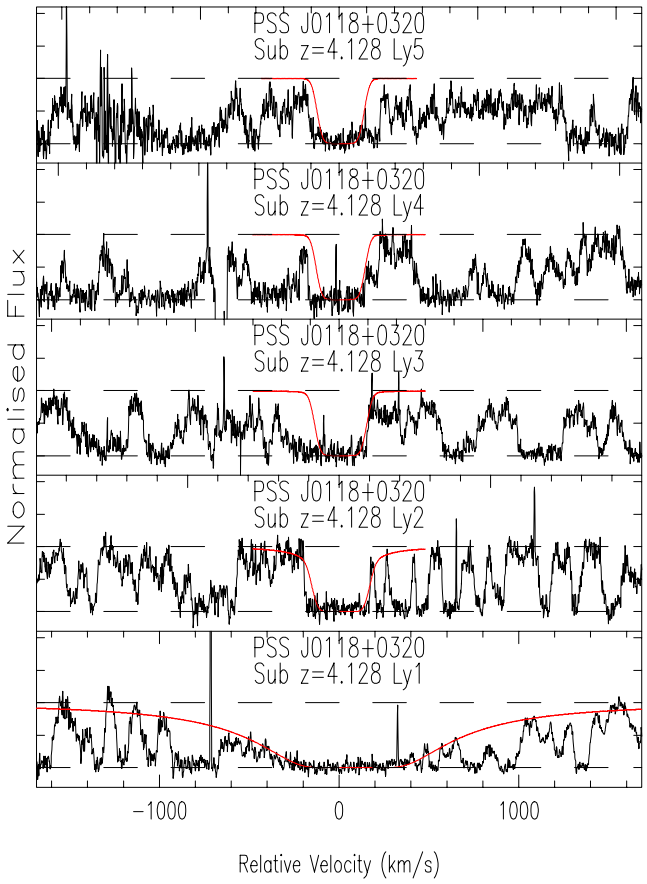

Figure 2. The absorber detected towards PSS J0118+0320 at $z_{\rm abs} = 4.128$ ($\log N_{\rm H\,I} = 20.02 \pm 0.15$).

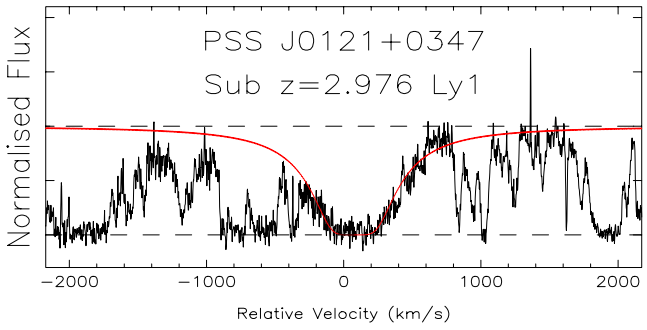

Figure 3. The absorber detected towards PSS J0121+0347 at $z_{\rm abs} = 2.976$ ($\log N_{\rm H\,I} = 19.53 \pm 0.10$).

systems are close by each other: they are separated by ∼5170 km s^{-1} with an additional $\log N_{\rm H\,I} < 19.0$ in between them (see second panel of Fig. 5, below). This group constitutes almost a multiple DLA (Lopez et al. 2001; Ellison & Lopez 2001; Lopez & Ellison 2003). In addition, we report the discovery of a further four sub-DLAs along the same line of sight. We measure $\log N_{\rm H\,I} = 19.01 \pm 0.10$ at $z_{\rm abs} = 3.139$, $\log N_{\rm H\,I} = 19.94 \pm 0.15$ at $z_{\rm abs} = 3.995$, $\log N_{\rm H\,I} = 19.16 \pm 0.15$ at $z_{\rm abs} = 3.999$ and $\log N_{\rm H\,I} = 19.09 \pm 0.15$ at $z_{\rm abs} = 4.021$. Again, two of these are very close to one another, $z_{\rm abs} = 3.995$ and 3.999 corresponding to 250 km s^{-1}. There are fitted together using Ly2 and Ly4 since those provide better constraints than Ly1. The Lyman series down to Ly4 is also available for

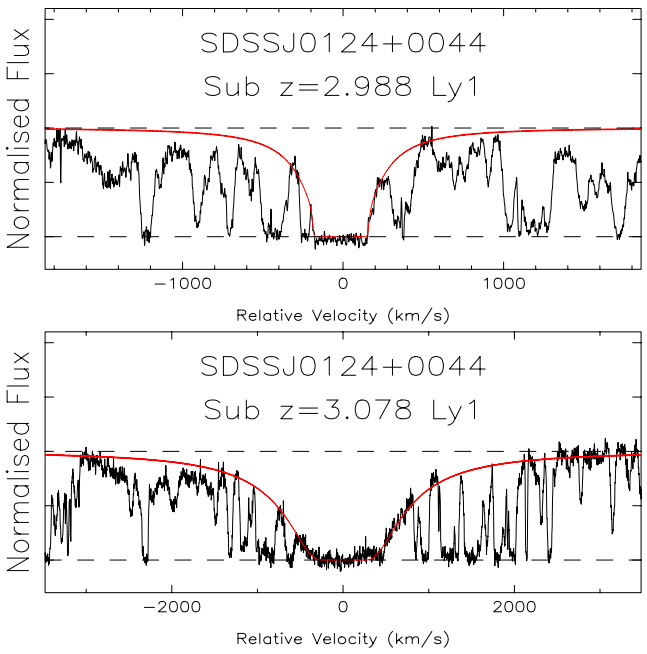

Figure 4. The absorbers detected towards SDSS J0124+0044 at $z_{\rm abs} = 2.988$ ($\log N_{\rm H\,I} = 19.18 \pm 0.10$) and $z_{\rm abs} = 3.078$ ($\log N_{\rm H\,I} = 20.21 \pm 0.10$).

the last three sub-DLAs. The various Lyman-series absorption lines along this rich line of sight are displayed in Fig. 5. Given the limited wavelength coverage of our spectrum, only metals associated with the lowest and the highest system are detected.

(vi) BRI J0137−4224 ($z_{\rm em} = 3.970$). Storrie-Lombardi et al. (2001) do not find any DLA in the spectrum of this quasar. We confirm that there are none of the highest H I column densities, but we find two sub-DLAs. The first system is at $z_{\rm abs} = 3.101$ and has an H I column density $\log N_{\rm H\,I} = 19.81 \pm 0.10$, while the second is at $z_{\rm abs} = 3.665$ and has $\log N_{\rm H\,I} = 19.11 \pm 0.10$. Both of these systems have metals associated with them. The Lyman series down to Ly11 is also visible for the second system. Fig. 6 shows the best Voigt profile-fitting solutions for these two systems.

(vii) PSS J0209+0517 ($z_{\rm em} = 4.174$). Péroux et al. (2001) report two DLAs in this quasar which were further confirmed by ESI/Keck II observations of Prochaska et al. (2003). Here, we measure $\log N_{\rm H\,I} = 20.47 \pm 0.10$ at $z_{\rm abs} = 3.666$ and $\log N_{\rm H\,I} = 20.45 \pm 0.15$ at $z_{\rm abs} = 3.863$ (Prochaska et al. measure $\log N_{\rm H\,I} = 20.55 \pm 0.10$ and $\log N_{\rm H\,I} = 20.55 \pm 0.10$ respectively). We also find a sub-DLA at $z_{\rm abs} = 3.707$. We measure $\log N_{\rm H\,I} = 19.24 \pm 0.10$ for that system. All these absorbers have metals associated with them. Fig. 7 shows our best fit of these H I lines.

(viii) BR J0244−0134 ($z_{\rm em} = 4.053$). This quasar was observed by Storrie-Lombardi, McMahon & Irwin (1996b) who did not report any DLA. The high-resolution spectrum that we have acquired shows that no sub-DLA is found either along this line of sight.

(ix) BR J0311−1722 ($z_{\rm em} = 4.039$). Péroux et al. (2001) report an absorber with column density below the classical definition along this line of sight from medium-resolution spectroscopy. Here, we confirm that the system has $\log N_{\rm H\,I} = 19.48 \pm 0.10$ at $z_{\rm abs} = 3.734$ observable down to Ly7 as shown in Fig. 8. Most of the constraints in this system come from Ly3 and Ly5. The lower members of the series were therefore merely used as a check for the solution. We

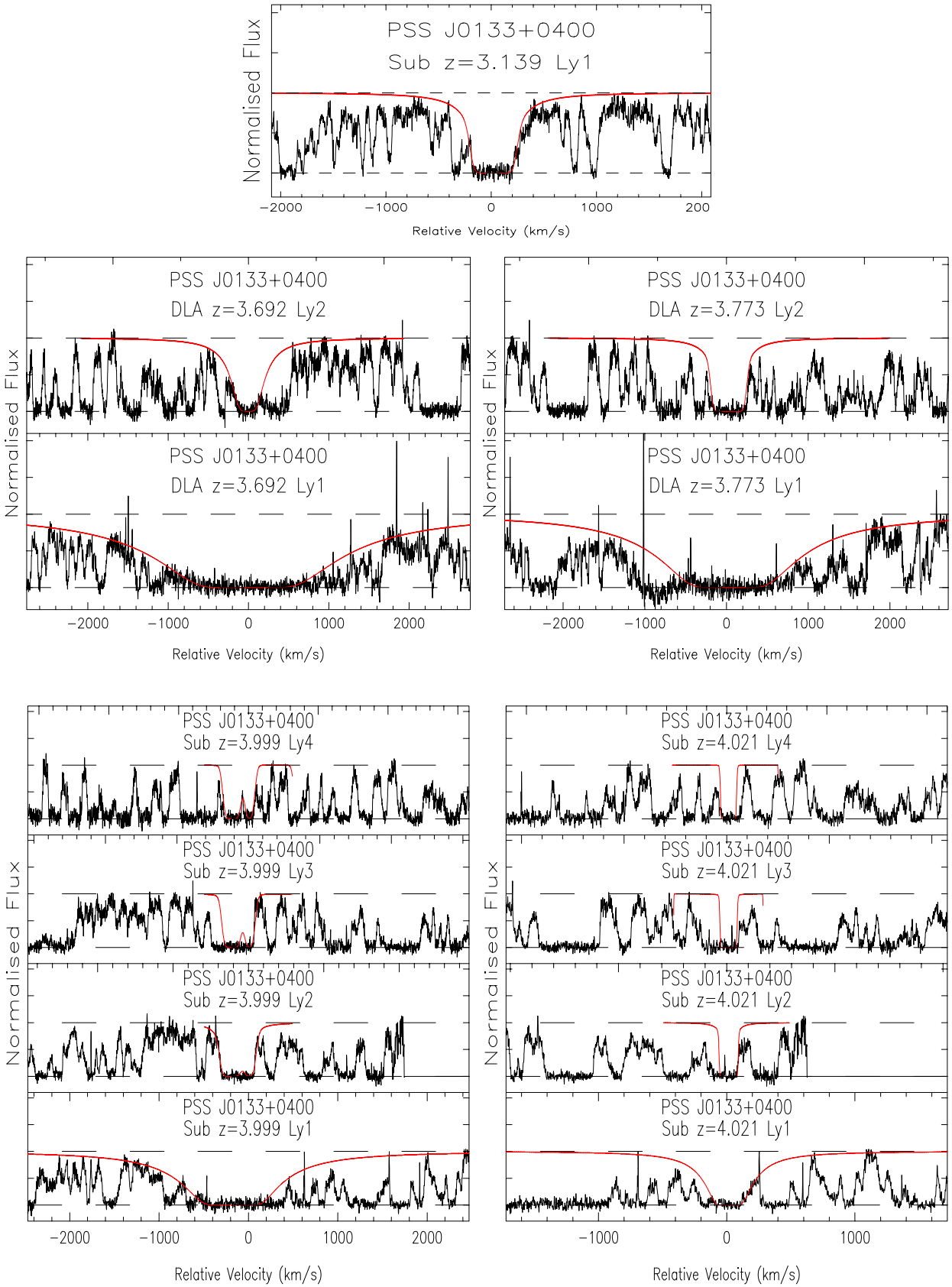

Figure 5. The rich line of sight towards PSS J0133+0400 is composed of systems with the following redshifts: $z_{\rm abs} = 3.139$ ($\log N_{\rm H\,I} = 19.01 \pm 0.10$), $z_{\rm abs} = 3.692$ ($\log N_{\rm H\,I} = 20.68 \pm 0.15$), $z_{\rm abs} = 3.773$ ($\log N_{\rm H\,I} = 20.42 \pm 0.10$), $z_{\rm abs} = 3.995$ ($\log N_{\rm H\,I} = 19.94 \pm 0.15$) together with $z_{\rm abs} = 3.999$ ($\log N_{\rm H\,I} = 19.16 \pm 0.15$) and finally $z_{\rm abs} = 4.021$ ($\log N_{\rm H\,I} = 19.09 \pm 0.15$).

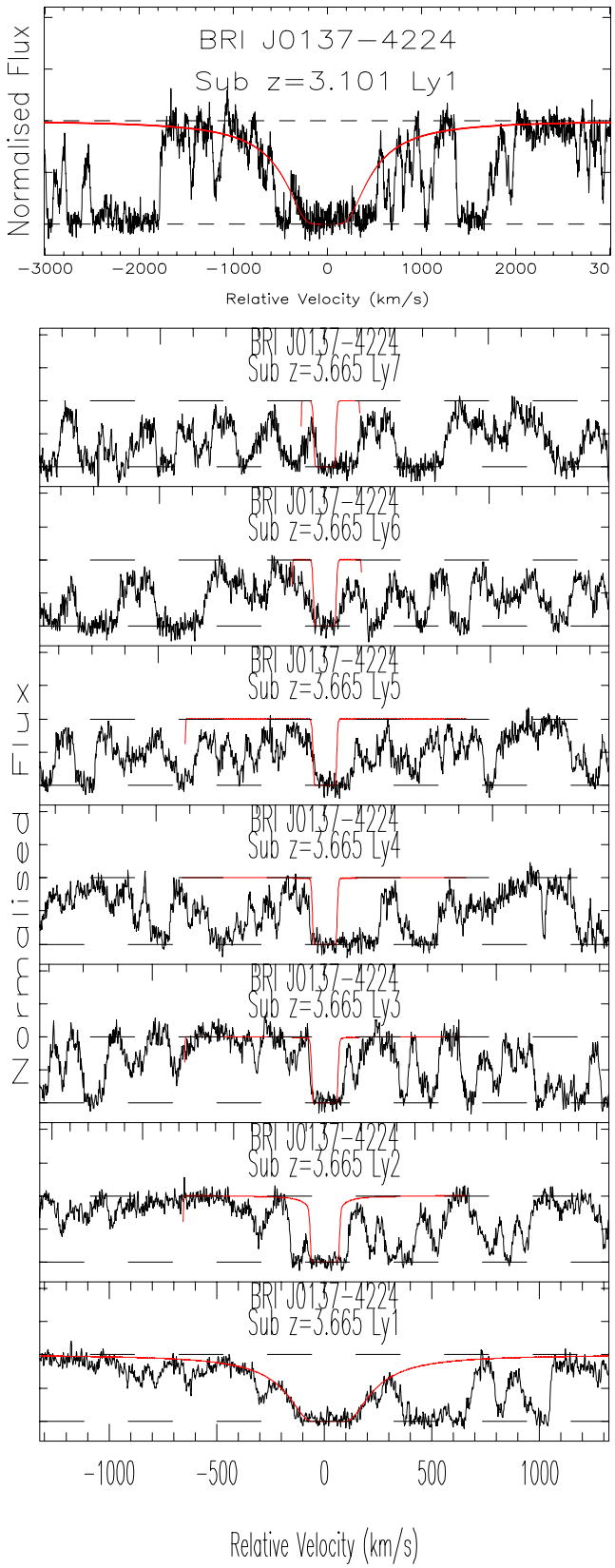

Figure 6. These are the two absorbers detected towards BRI J0137−4224 at $z_{\rm abs} = 3.101$ ($\log N_{\rm H\,I} = 19.81 \pm 0.10$) and $z_{\rm abs} = 3.665$ ($\log N_{\rm H\,I} = 19.11 \pm 0.10$). The latter system is detected down to Ly11, but for display purposes only the first seven members of the series are shown.

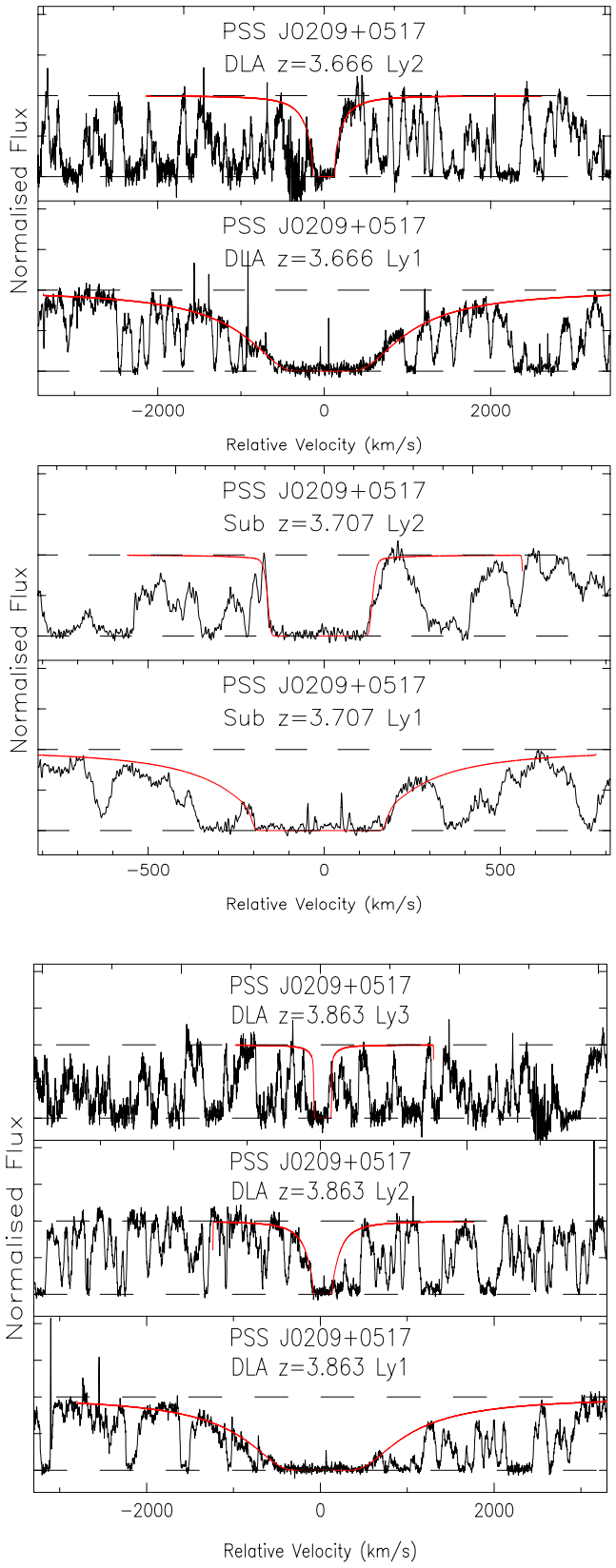

Figure 7. The absorbers detected towards PSS J0209+0517 at $z_{\rm abs} = 3.666$ ($\log N_{\rm H\,I} = 20.47 \pm 0.10$), $z_{\rm abs} = 3.707$ ($\log N_{\rm H\,I} = 20.55 \pm 0.10$) and $z_{\rm abs} = 3.863$ ($\log N_{\rm H\,I} = 20.45 \pm 0.15$).

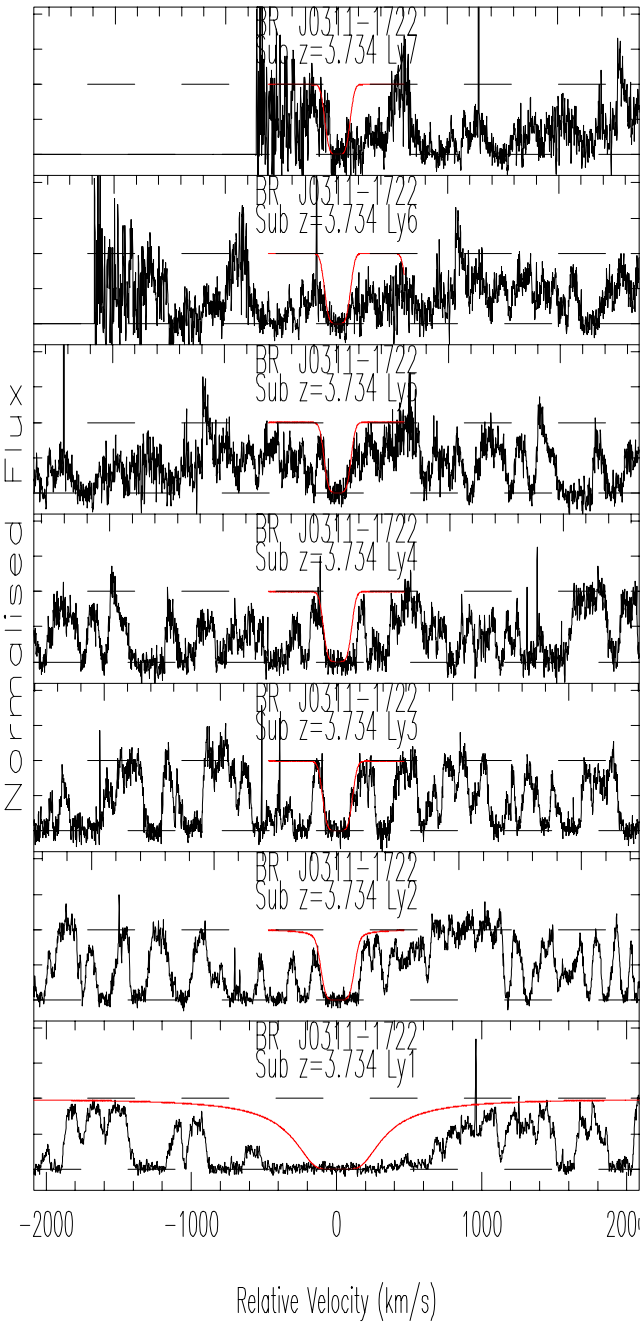

Figure 8. The absorber detected towards BR J0311−1722 at $z_{\rm abs} = 3.734$ ($\log N_{\rm H\,I} = 19.48 \pm 0.10$).

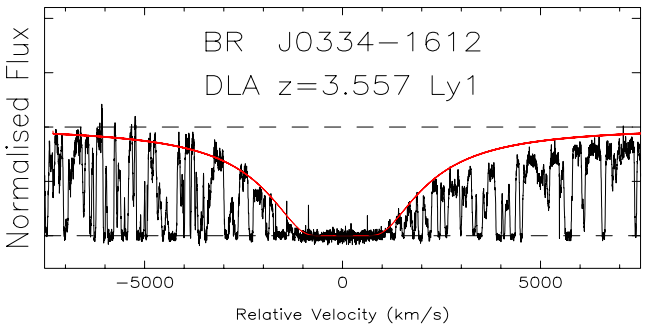

Figure 9. The DLA absorber detected towards BR J0334−1612 with $z_{\rm abs} = 3.557$ ($\log N_{\rm H\,I} = 21.12 \pm 0.15$). We note the asymmetry in the shape of the profile, a possible signature of multi-component absorbers.

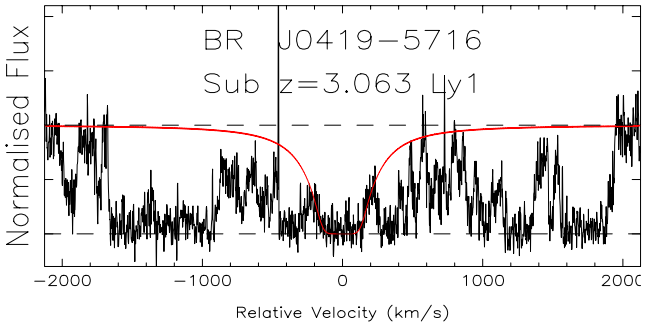

Figure 10. The sub-DLA absorber detected towards BR J0419−5716 at $z_{\rm abs} = 3.063$ ($\log N_{\rm H\,I} = 19.17 \pm 0.10$).

note that using only Ly1 to fit this system would mistakenly derive a much higher H I (>20.0). Metals are found at the same redshift.

(x) BR J0334−1612 ($z_{\rm em} = 4.363$). A DLA at $z_{\rm abs} = 3.56$ was reported by Péroux et al. (2001) from medium-resolution spectroscopy. They derive $\log N_{\rm H\,I} = 21.0$ in excellent agreement with the measurement made here from higher resolution spectroscopy: $\log N_{\rm H\,I} = 21.12 \pm 0.15$ with $z_{\rm abs} = 3.557$. Nevertheless, we note the asymmetry in the shape of the profile, a possible signature of multi-component absorbers. Metal lines associated with this system are detected in the red part of the spectrum. Fig. 9 shows our best fit of this H I line. We also note in the spectrum of this quasar a real and significant broad dip in the continuum at $\lambda \sim 5200$ Å. This cannot be explained by any known broad absorption lines, nor by any ions at the emission redshift and does not correspond to the beginning of the Lymanβ forest either. Similar features (although not as dramatic) have been reported by Levshakov et al. (2004). In that case, the dips are clearly associated with O VI at the emission redshift and are interpreted as ejected material or intracluster cooling flow.

(xi) BR J0419−5716 ($z_{\rm em} = 4.461$). This quasar was observed by Péroux et al. (2001) who did not detect any sub-DLA in its medium resolution spectrum. Using higher-resolution data, we detect a sub-DLA with $z_{\rm abs} = 3.063$ with $\log N_{\rm H\,I} = 19.17 \pm 0.10$ as well as one metal transition. Fig. 10 shows our best fit of this H I line.

(xii) BR J2017−4019 ($z_{\rm em} = 4.131$). This quasar is a Broad Absorption Line (BAL) quasar (Péroux et al. 2001). We carefully searched for DLA/sub-DLAs in the regions free from BAL features but did not detect any. We note, however, O VI λλ1032 and 1037 features at $z_{\rm abs} = 3.9966$, 3.9692 and maybe also at $z_{\rm abs} = 3.7300$.

(xiii) PSS J2154+0335 ($z_{\rm em} = 4.363$). This quasar was observed by Péroux et al. (2001) who report a DLA at $z_{\rm abs} = 3.61$. This system falls in the setting gap of our UVES spectra. On the other hand, we discover a new sub-DLA at $z_{\rm abs} = 3.177$ with $\log N_{\rm H\,I} = 19.23 \pm 0.15$. No metals were found associated with system over the limited wavelength range of our spectrum. Fig. 11 shows our best fit of this H I line.

(xiv) BR J2215−1611 ($z_{\rm em} = 3.990$). This quasar was observed by Storrie-Lombardi et al. (1996b) who did not find any DLA in the spectrum. Here we report on two new sub-DLAs with $\log N_{\rm H\,I} = 19.01 \pm 0.15$ and 20.05 ± 0.15 at $z_{\rm abs} = 3.656$ and 3.662 respectively. The two are separated by just ∼320 km s^{-1}. The Lyman series is detected down to Ly3, where the division into two distinct systems is unambiguous. Several metal lines are detected at these

redshifts too. Fig. 12 shows our best fit of these H I lines. We also note O VI λλ1032 and 1037 features at $z_{\rm abs} = 3.9785$ along this quasar line of sight.

(xv) BR J2216−6714 ($z_{\rm em} = 4.469$). This quasar was observed by Péroux et al. (2001) who do not report an absorber but do mention a possible sub-DLA candidate at $z_{\rm abs} = 3.37$. We now confirm that system and derive $\log N_{\rm H\,I} = 19.80 \pm 0.10$ at $z_{\rm abs} = 3.368$. Several metal lines are also observed at this redshift. Fig. 13 shows our best fit of this H I line.

(xvi) BR J2239−0552 ($z_{\rm em} = 4.558$). This quasar was observed by Storrie-Lombardi et al. (1996b) who report a DLA at $z_{\rm abs} = 4.08$. We now confirm that system and derive $\log N_{\rm H\,I} = 20.55 \pm 0.10$ at $z_{\rm abs} = 4.079$ in good agreement with estimates from medium-resolution spectroscopy. The absorber is detected down to the Ly3 level and has associated metal lines. Fig. 14 shows our best fit of these H I lines.

(xvii) BR J2349−3712 ($z_{\rm em} = 4.208$). This quasar was observed by Péroux et al. (2001) at medium resolution. They do not find any DLA along its line of sight. Here, we report on the discovery of three sub-DLAs, two of which are blended. The first system has $\log N_{\rm H\,I} = 19.12 \pm 0.10$ at $z_{\rm abs} = 3.581$ while the two others have $\log N_{\rm H\,I} = 19.79 \pm 0.15$ at $z_{\rm abs} = 3.690$ and $\log N_{\rm H\,I} = 19.78 \pm 0.10$ at $z_{\rm abs} = 3.696$ (i.e. $\Delta v \sim 380$ km s^{-1}). The subdivision of these is unambiguous in Ly2. For all the systems the Lyman series is available down to Ly3. No associated metal lines are detected over the limited wavelength coverage of our spectrum. Fig. 15 shows our best fit of these H I lines.

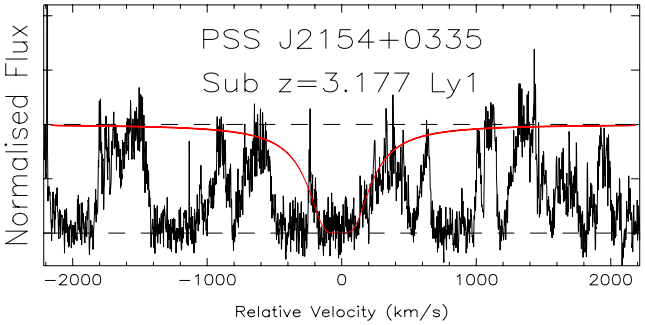

Figure 11. The sub-DLA absorber detected towards PSS J2154+0335 at $z_{\rm abs} = 3.177$ ($\log N_{\rm H\,I} = 19.23 \pm 0.15$).

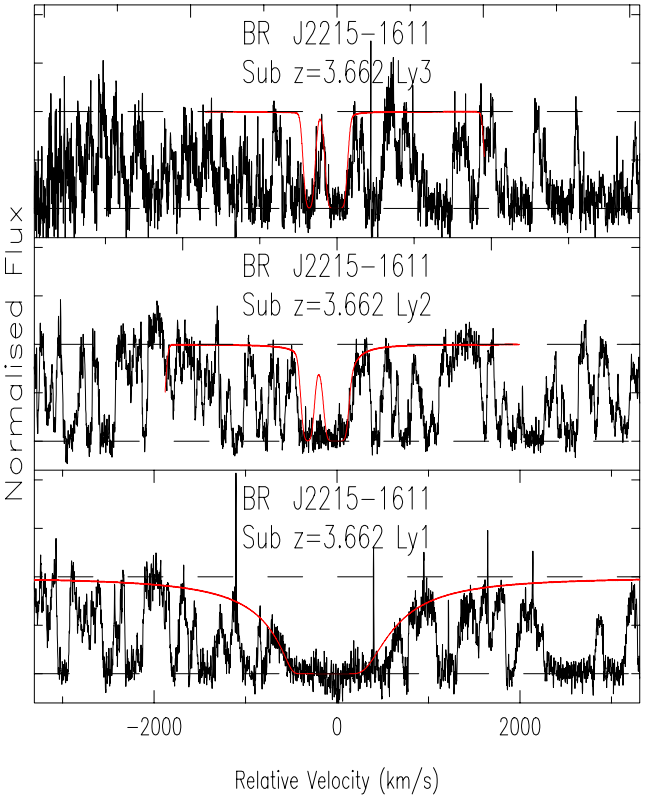

Figure 12. The sub-DLA absorbers detected towards BR J2215−1611 at $z_{\rm abs} = 3.656$ ($\log N_{\rm H\,I} = 19.01 \pm 0.15$) and $z_{\rm abs} = 3.662$ ($\log N_{\rm H\,I} = 20.05 \pm 0.15$) respectively.

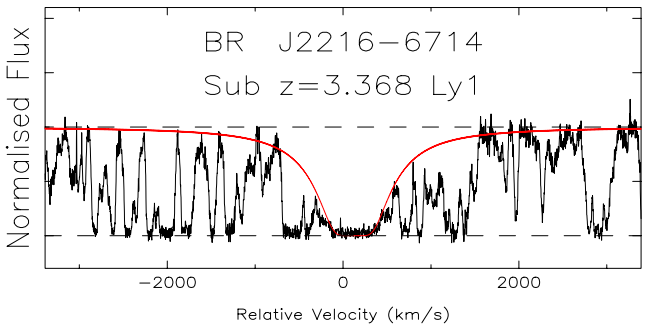

Figure 13. The sub-DLA absorber detected towards BR J2216−6714 at $z_{\rm abs} = 3.368$ ($\log N_{\rm H\,I} = 19.80 \pm 0.10$).

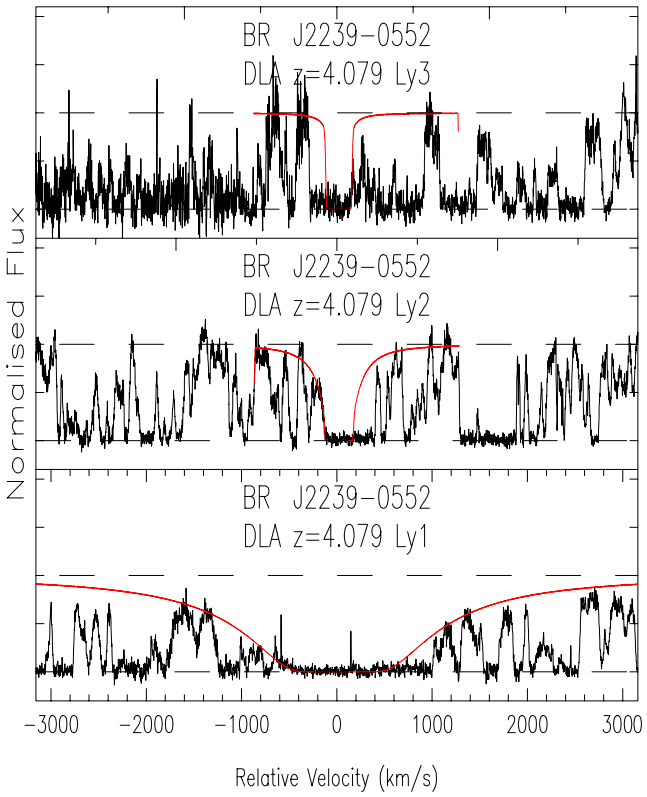

Figure 14. The DLA absorber detected towards BR J2239−0552 at $z_{\rm abs} = 4.079$ ($\log N_{\rm H\,I} = 20.55 \pm 0.10$).

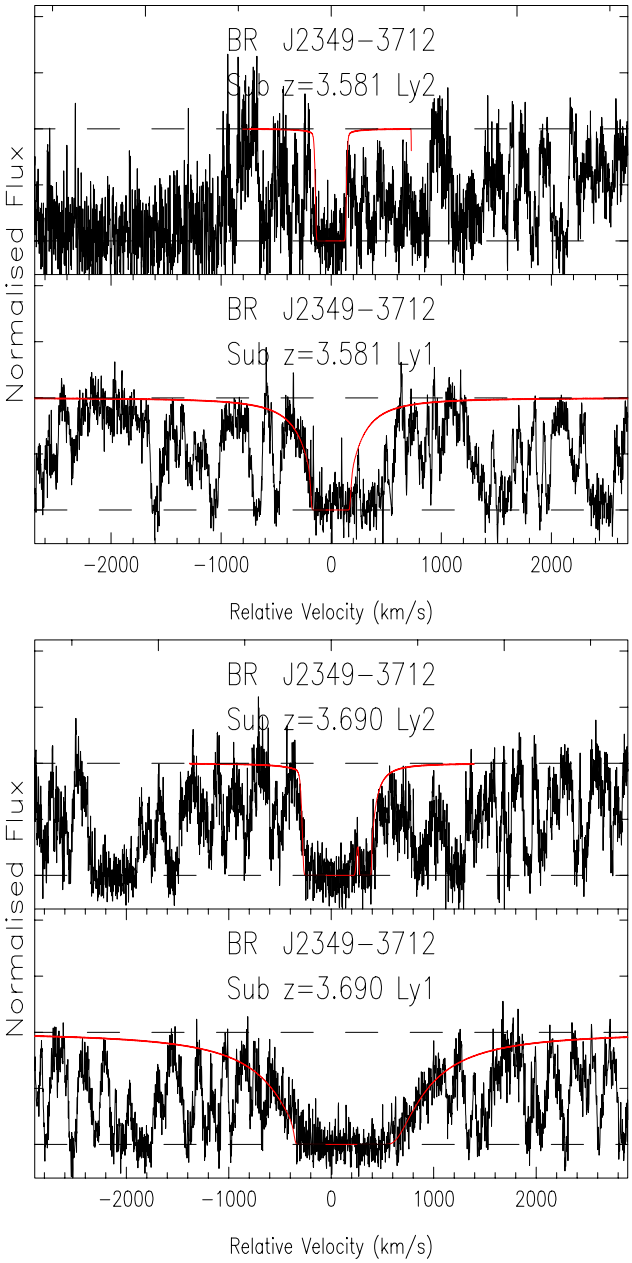

Figure 15. The sub-DLA absorbers detected towards BR J2349−3712 at $z_{\rm abs} = 3.581$ ($\log N_{\rm H\,I} = 19.12 \pm 0.10$) while the two others are at $z_{\rm abs} = 3.690$ ($\log N_{\rm H\,I} = 19.79 \pm 0.15$) and $z_{\rm abs} = 3.696$ ($\log N_{\rm H\,I} = 19.78 \pm 0.10$).

2.4 Medium/high-resolution $N_{\rm H\,I}$ comparison

Seven of the quasar absorbers described above are classical DLAs with $\log N_{\rm H\,I} > 20.3$. In Table 3, the $N_{\rm H\,I}$ column density estimates from medium-resolution spectroscopy of these DLAs is compared with the new high-resolution measurements presented here. The last two systems (toward BR J0334−1612 and BR J2239−0552) were also observed by Storrie-Lombardi & Wolfe (2000) who found $N_{\rm H\,I}$ values in very good agreement with ours. The comparison shows that previous $N_{\rm H\,I}$ estimates from 5-Å resolution quasar spectra are reliable. In fact, it is also known that estimates of systems with high column density from echelle data might be affected by the difficulty of tracing the correct continuum over a different echelle order. In the sub-DLA regime however, high-resolution spectra are definitely required in order to accurately measure $N_{\rm H\,I}$.

Table 3. This table compiles the DLA column density and redshift estimates from 5 Å (full width at half maximum), S/N per pixel ∼20 (Péroux et al. 2001, except BR J2239−0552 which is from Storrie-Lombardi et al. 1996b) and 2 Å, S/N per pixel ∼25 quasar spectra from the present study.

Quasar	medium resolution		high resolution		$\Delta N_{\rm H\,I}$
	$z_{\rm abs}$	$N_{\rm H\,I}$	$z_{\rm abs}$	$N_{\rm H\,I}$	(med-high)
BR J0006−6208	3.20	20.9	3.202	20.80	+0.10
PSS J0133+0400	3.69	20.4	3.692	20.68	+0.28
...	3.77	20.5	3.773	20.42	−0.08
PSS J0209+0517	3.66	20.3	3.666	20.47	+0.17
...	3.86	20.6	3.863	20.43	−0.17
BR J0334−1612	3.56	21.0	3.557	21.12	+0.12
BR J2239−0552	4.08	20.4	4.079	20.55	+0.15
mean	3.69	20.58	3.689	20.64	+0.08
min value	3.20	20.30	3.202	20.42	−0.17
max value	4.08	21.00	4.079	21.12	+0.28

3 ANALYSIS

3.1 Properties of the survey

3.1.1 Survey sensitivity

Table 4 lists the minimum ($z_{\rm min}$) and maximum ($z_{\rm max}$) redshifts along which a sub-DLA could be detected along each quasar line-of-sight. $z_{\rm min}$ corresponds to the point below which the S/N is too low to find absorption features at the sub-DLA threshold of $W_{\rm rest} = 2.5$ Å, and $z_{\rm max}$ is 3000 km s^{-1} blueward of the Lyα emission of the quasar. We took care to exclude the DLA regions and the gaps in the spectrum due to non-overlapping UVES settings when computing the redshift path surveyed.

Fig. 16 shows the cumulative number of lines of sight along which a sub-DLA *could* have been detected at the 5σ confidence level. This survey sensitivity, $g(z)$, is defined by:

$$g(z) = \sum H\left(z_i^{\rm max} - z\right) H\left(z - z_i^{\rm min}\right) \quad (1)$$

where H is the Heaviside step function. In Fig. 16, it is compared with those of the previous sub-DLA survey (Péroux et al. 2003b). It shows that our new observations probe a higher redshift interval than did the first archive-based work and that the combination of the two provides more homogeneous survey coverage in the range $z = 1.5$ to 4.5.

3.1.2 Redshift distribution

The sub-DLA sample described in Section 2 leads to 21 sub-DLAs along 17 quasar lines of sight, whilst we had 10 sub-DLAs making up our 'statistical sample' toward 22 lower redshift quasars in our previous archival study (Dessauges-Zavadsky et al. 2003). We also confirm the presence of seven DLAs along the same lines of sight. The histograms showing the redshift distribution of these homogeneous sub-DLA samples are shown in Fig. 17.

3.2 Sub-DLAs statistical properties

3.2.1 Redshift number density

The number of quasar absorbers per unit redshift, $n(z)$, is a direct observable. This quantity, however, can be used to constrain the evolution or lack of it only when deconvolved from the effect of cosmology.

Table 4. Redshift path surveyed. $z_{\rm min}$ corresponds to the point below which no flux is observed and $z_{\rm max}$ is 3000 km s^{-1} bluewards of the Lyα emission line. Gap in non-overlapping settings and known DLAs are taken into account.

Quasar	$z_{\rm em}$	$z_{\rm min}$	$z_{\rm max}$
BR J0006−6208	4.455	3.083	3.188
...	...	3.216	3.732
...	...	3.798	4.450
PSS J0118+0320	4.230	2.767	4.225
PSS J0121+0347	4.127	2.739	3.410
...	...	3.474	4.122
SDSS J0124+0044	3.840	2.414	3.835
PSS J0133+0400	4.154	2.414	3.247
...	...	3.305	3.676
...	...	3.707	3.765
...	...	3.786	4.149
BRI J0137−4224	3.970	2.344	3.965
PSS J0209+0517	4.174	2.767	3.658
...	...	3.675	3.855
...	...	3.872	4.169
BRI J0244−0134	4.053	2.414	3.247
...	...	3.305	4.048
BR J0311−1722	4.039	2.560	3.410
...	...	3.474	4.034
BR J0334−1612	4.363	2.748	3.541
...	...	3.573	4.358
BR J0419−5716	4.461	2.748	3.572
...	...	3.639	4.456
BR J2017−4019	4.131	2.607	2.994
...	...	3.022	3.407
...	...	3.473	4.126
PSS J2154+0335	4.363	2.748	3.572
...	...	3.639	4.358
BR J2215−1611	3.990	2.315	3.408
...	...	3.473	3.985
BR J2216−6714	4.469	2.748	4.464
BR J2239−0552	4.558	2.894	3.735
...	...	3.801	4.070
...	...	4.096	4.552
BR J2349−3712	4.208	2.601	3.407
...	...	3.473	4.203

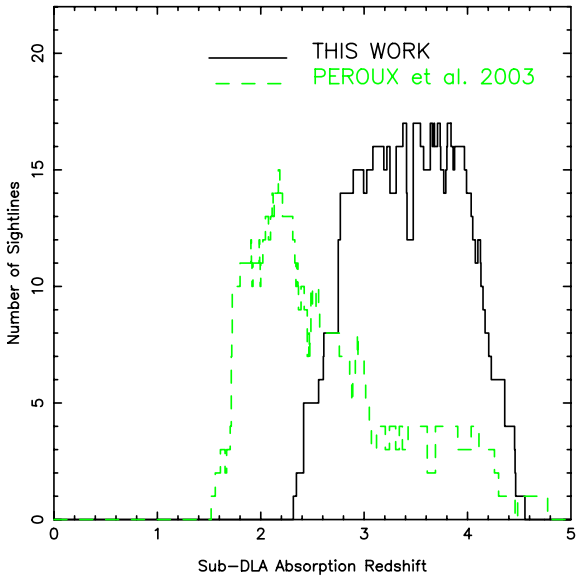

Figure 16. Survey sensitivity function. The g(z) function shows the cumulative number of lines of sight along which a sub-DLA system could be detected. The light grey histogram represents our archival search (Péroux et al. 2003b) while the present work is represented in black. It shows that our new observations probe a higher redshift interval than the archival work. The dip at $z \sim 3.45$ corresponds to the five quasars for which the gap in the 540 setting was not covered.

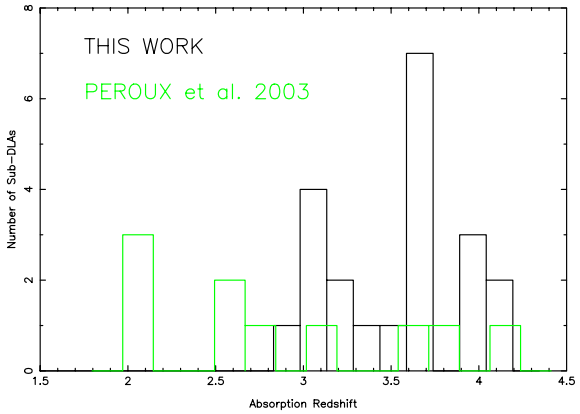

Figure 17. Histogram of the redshift distribution of the sub-DLAs discovered as part of this survey. Péroux et al. (2003b) refers to the statistical sample of the archival search undertaken at lower redshift (grey histogram). The black histogram represents the new high-redshift sample from the present study.

The data acquired here, used in combination with recent results from the literature, allow us to determine this quantity for various classes of quasar absorbers. This is shown in Fig. 18 where the number density for DLAs (Péroux et al. 2003a; Rao, Turnshek & Nestor, in preparation), sub-DLAs (both predictions from Péroux et al. 2003a, computation and new direct measurements from the present work) and LLS are presented (also from Péroux et al. 2003a). It can already be seen that the predictions overestimated the number of sub-DLAs at $z > 4$ while they underestimated the number of such systems at $z < 3.5$. The observations show that the number density of sub-DLAs is flatter than expected. All these observations are tabulated in Table 5. Assuming no evolution in the number density, Φ or gas cross-section σ, the lack of evolution in the redshift number density in a non-zero Λ-Universe can be expressed as (see for example Péroux et al. 2004a):

$$n(z) = n_0(1+z)^2 \left[\frac{H(z)}{H_0}\right]^{-1} \quad (2)$$

where

$$\frac{H(z)}{H_0} = \left\{\Omega_{\rm M} z(1+z)^2 - \Omega_\Lambda[z(z+2)] + (1+z)^2\right\}^{1/2}, \quad (3)$$

where $\Omega_{\rm M}$ is the matter density and Ω_Λ is the contribution of the cosmological constant. The following values have been used: $\Omega_{\rm M} = 0.3$, $\Omega_\Lambda = 0.7$ and $H_0 = 0.65$. These 'no-evolution curves' are shown for each class of quasar absorbers in Fig. 18 where n_0 is taken to be $n(z = 0) = 0.045 \pm 0.006$ derived by Zwaan et al. (2005b) from high-resolution 21-cm emission line observations of the $z = 0$ analogues of DLAs. The other curves are scaled according to a factor representative of the difference in redshift number density of sub-DLAs and LLS in the redshift range $2.5 < z < 3.0$. Departure from 'no evolution' at $z \geqslant 3$ is clear for all classes of quasar absorbers. For comparison with previous work, the

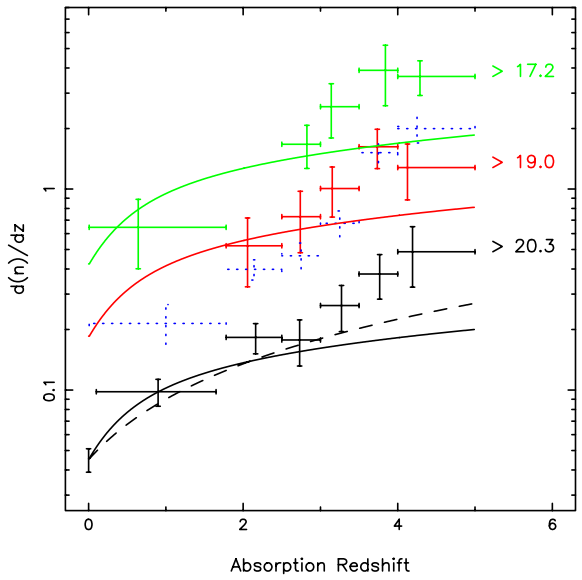

Figure 18. Number density of various classes of quasar absorbers as a function of redshift taken from Péroux et al. (2003a) and Rao et al. (in preparation) except for sub-DLAs (this work). The horizontal error bars are the bin sizes and the vertical error bars are the 1σ uncertainties. The dotted bins are the predictions of the number density of sub-DLAs from Péroux et al. (2003a), while the light grey bins at $\log N_{\rm H\,I} > 19.0$ correspond to the observed number density presented in this paper. The DLAs $n(z=0)$ data point is from the 21-cm emission line observations of Zwaan et al. (2005b). The curves represent a non-evolving population for a non-zero Λ-Universe except for the dashed line which is for a $\Lambda = 0, q_0 = 0$ Universe.

dashed line shows the non-evolving population for a $\Lambda = 0, q_0 = 0$ Universe.

3.2.2 *Size of quasar absorbers*

With the assumption that all classes of absorbers (i.e. DLAs, sub-DLAs and LLS) and all members of a given class are arising from the same underlying parent population, one can estimate the cross-section radius of spherical absorbers, σ, from the observed redshift number density $n(z)$. Following Tytler (1981) and using a non-zero Λ-cosmology, we find:

$$n(z) = \frac{c}{H_0}(1+z)^2 \left[\frac{H(z)}{H_0}\right]^{-1} \int_0^\infty \epsilon \Phi(L) \kappa \pi R^2(L)\, {\rm d}(L), \qquad (4)$$

where $R(L)$ is the average H I absorption cross-section radius of a spherical galaxy with luminosity L, and ϵ is the fraction of galaxies which have gaseous absorbing envelopes with filling factor κ. $\Phi(L)$ is estimated from the Schechter (1976) galaxy luminosity function:

$$\Phi\left(\frac{L}{L_*}\right) = \Phi_* \left(\frac{L}{L_*}\right)^{-s} \exp\left(\frac{L}{L_*}\right). \qquad (5)$$

If we further assume that a Holmberg (1975) relation between optical radius and luminosity holds at all redshifts

$$\frac{R}{R_*} = \left(\frac{L}{L_*}\right)^t, \qquad (6)$$

we obtain the following relation for the radius:

$$R_*^{-2} = \frac{c}{H_0}\frac{(1+z)^2}{n(z)}\left[\frac{H(z)}{H_0}\right]^{-1} \epsilon \Phi_* \kappa \pi \Gamma(1+2t-s), \qquad (7)$$

where $\Gamma(x)$ is the Gamma function. We take $\epsilon = 1, \kappa = 1$ and $t = 0.4$ (derived from Peterson, Strom & Strom 1979). Two different sets of parameters are used for the luminosity function: $\Phi_* = 0.0149 \pm 0.04$ h^3 Mpc^{-3} and $s = 1.05 \pm 0.01$ for $z < 0.75$ from the Sloan measurements of Blanton et al. (2003) and $\Phi_* = 0.0142^{+0.0015}_{-0.0013}$ h^3 Mpc^{-3} and $s = 0.50^{+0.08}_{-0.06}$ for $z > 0.75$ from infrared selected galaxies of Chen et al. (2003). These yield an H I gas radius of

$$R_* = A h_{100}^{-1} \frac{n(z)^{1/2}}{(1+z)}\left[\frac{H(z)}{H_0}\right]^{1/2} \ [\rm kpc], \qquad (8)$$

where $A = 76$ for $z < 0.75$ and $A = 91$ for $z > 0.75$. The redshift evolution of the characteristic radius of DLAs, sub-DLAs and LLS are plotted in Fig. 19. All classes of absorbers have their characteristic radius, R_*, decreasing with decreasing redshift, and this effect is stronger at lower column densities. For comparison, the impact parameters of spectroscopically confirmed $z < 1$ DLAs (see Boissier, Péroux & Pettini 2003, for a compilation) and MgII-selected galaxies (Steidel et al. 2002), a proxy for LLS, are also plotted. Given the number of assumptions made in the calculation, the few available observations are in relatively good agreement with our results.

3.2.3 *Column density distribution*

The differential column density distribution describes the evolution of quasar absorbers as a function of column density and redshift. It

Table 5. This table summarizes the observed number density of quasar absorbers for different column-density ranges together with the predicted number density of sub-DLAs (from Péroux et al. 2003a and Rao et al., in preparation, except for the sub-DLA number density which is from the present work). The empty entries are regions of redshift/column-density parameter space as yet unobserved. Column headings are as follows: #: number of absorption systems. $19.0^*_{\rm obs}$: #, $\langle z\rangle$ and dz refer to systems with $19.0 < \log N_{\rm H\,I} < 20.3$, whilst $n(z)$ is for all systems with $\log N_{\rm H\,I} > 19.0$.

$\log N_{\rm H\,I}$			>17.2				>19.0$^*_{\rm obs}$		>19.0$_{\rm pred}$			>20.3	
z range	#	$\langle z\rangle$	dz	$n(z)$	#	$\langle z\rangle$	dz	$n(z)$	$n(z)$	#	$\langle z\rangle$	dz	$n(z)$
0.01−1.78	7	0.64	10.9	0.64±0.24	..	...	...	...	0.21	n/a	0.90	n/a	0.10±0.02
1.78−2.50	..	...	...	...	3	2.06	8.8	0.52±0.20	0.40	34	2.16	186.1	0.18±0.03
2.50−3.00	17	2.82	10.2	1.67±0.41	5	2.74	9.1	0.73±0.25	0.46	15	2.73	84.5	0.18±0.05
3.00−3.50	11	3.14	4.3	2.57±0.77	7	3.15	9.4	1.01±0.28	0.67	15	3.27	57.0	0.26±0.07
3.50−4.00	9	3.84	2.3	3.89±1.30	12	3.74	9.6	1.62±0.36	1.52	16	3.77	42.4	0.38±0.09
4.00−5.00	26	4.29	7.2	3.63±0.71	4	4.13	5.1	1.28±0.40	2.00	9	4.19	18.5	0.49±0.16
total	71	...	34.9	...	31	...	42.0	...	...	100	...	514.8	...

n/a: 'not applicable' refers to low-redshift Mg II-selected systems and so the number of absorption systems and corresponding dz are not directly comparable to higher-redshift statistics.

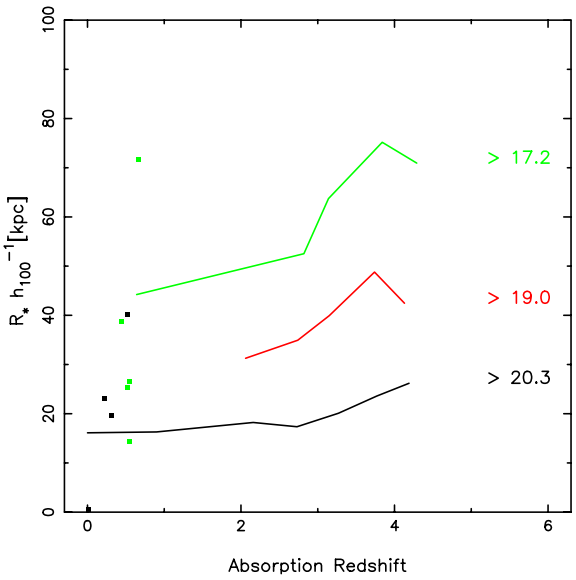

Figure 19. The redshift evolution of the characteristic radius, R_*, of DLAs, sub-DLAs and LLS. For comparison, the impact parameters of spectroscopically confirmed $z < 1$ DLAs (see Boissier et al. 2003 for a compilation) and MgII-selected galaxies (Steidel et al. 2002), a proxy for LLS, are also plotted.

is defined as:

$$f(N, z)\,\mathrm{d}N\,\mathrm{d}X = \frac{n}{\Delta N \sum_{i=1}^{m} \Delta X_i}\,\mathrm{d}N\,\mathrm{d}X \qquad (9)$$

where n is the number of quasar absorbers observed in a column density bin $[N, N + \Delta N]$ obtained from the observation of m quasar spectra with total absorption distance coverage $\sum_{i=1}^{m} \Delta X_i$. The column density distribution for two redshift ranges, $z < 3.5$ and $z > 3.5$ are shown in Fig. 20. These redshifts are chosen to allow a direct comparison with the work of Péroux et al. (2003a). In particular, the highest redshift is set to $z = 5$ to match DLA surveys even though the sub-DLA search is made only up to $z = 4.5$ (see Fig. 16). Again, the observations (solid bins) are compared with the predictions from Péroux et al. (2003a). The new data allow us to determine $f(N, z)$ down to $\log N_{\rm H\,I} = 19.0$. The column density distribution has often been fitted with a simple power law (i.e. Prochaska & Herbert-Fort 2004), but there has been recent work showing that a Schechter-type of function is more appropriate (Pei & Fall 1995; Storrie-Lombardi et al. 1996b; Péroux et al. 2003a). In any case, it should be noted that *neither* of these two functions is physically motivated; rather, they are chosen so as to best describe the data. However, as more observations are available, a clear departure from the power law is observed. This flattening of the distribution in the sub-DLA regime is indeed expected as the quasar absorbers become less self-shielded and part of their neutral gas is ionized by incident UV flux. We note once more the paucity of very high column-density DLAs at high redshift. All the data are summarized in Table 6.

3.3 $\Omega_{\rm H\,I+He\,II}$ gas mass

3.3.1 Cumulative number of absorbers

In Fig. 21, the number of quasar absorbers per unit comoving distance interval is plotted as a function of $\log N_{\rm H\,I}$. The new observations increase, by one dex, the $N_{\rm H\,I}$ column-density parameter space probed and therefore provide a much better handle on the true shape of the distribution. This, in turn, is crucial for constraining the total H I gas content which is a function of both column densities and redshifts. In our surveys, the DLA and sub-DLA samples (and associated redshift paths) are totally *independent* (Fig. 21) in the sense that the quasars used to make up the samples are different in both cases given that higher resolution is required for the study of sub-DLAs. Therefore, the shapes of both sections of the curves are unrelated and the fact that the function in the sub-DLA regime is a smooth continuation of the DLA part is a result of the observations.

3.3.2 $\Omega_{\rm H\,I+He\,II}$

The gas mass density, $\Omega_{\rm H\,I+He\,II}$, observed in high-redshift quasar absorbers is classically expressed as a fraction of today's critical

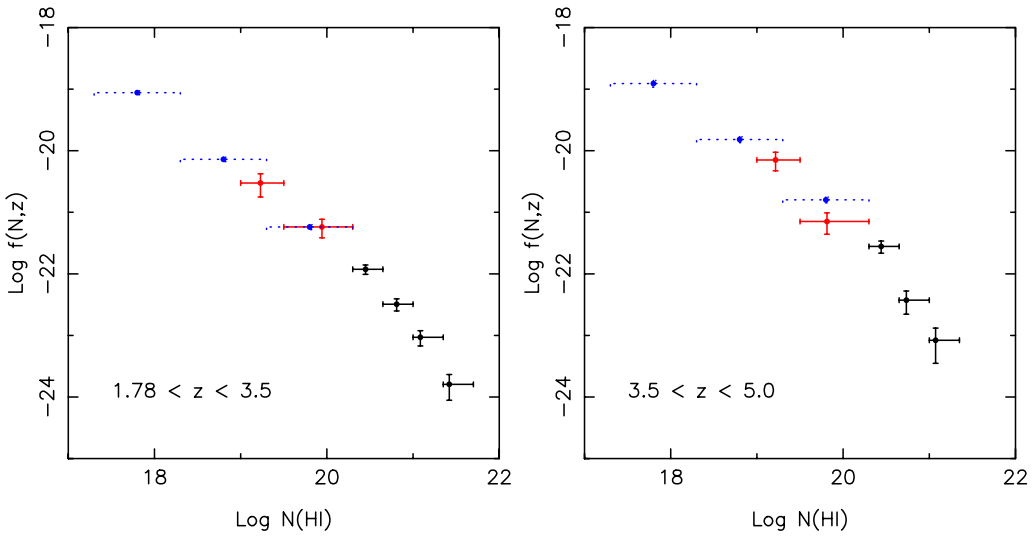

Figure 20. Column-density distributions for two redshift ranges down to the sub-DLA definition. The horizontal error bars are the bin sizes and the vertical error bars represent the uncertainties. The dotted bins are the predictions from fitting a Schechter function to the expected number of LLS (Péroux et al. 2003a), while the two solid bins at $19.0 < \log N_{\rm H\,I} < 20.3$ correspond to the direct observations from the sample of sub-DLAs presented here.

Table 6. This table summarizes the observed column-density distribution of quasar absorbers down to the sub-DLA column density. The empty entry in the highest column density bin at the highest redshift range reflects the lack of systems with $\log N_{\rm H\,I} > 21.35$ at $z > 3.5$.

z range		1.78−3.5					3.5−5.0			
$\log N_{\rm H\,I}$ range	#	log $\langle N_{\rm H\,I}\rangle$	log $f(N,z)$	log $f_{\rm min}(N,z)$	log $f_{\rm max}(N,z)$	#	log $\langle N_{\rm H\,I}\rangle$	log $f(N,z)$	log $f_{\rm min}(N,z)$	log $f_{\rm max}(N,z)$
19.00−19.50	6	19.23	−20.5	−20.4	−20.8	9	19.22	−20.2	−20.0	−20.3
19.50−20.30	9	19.94	−21.2	−21.1	−21.4	7	19.81	−21.1	−21.0	−21.4
20.30−20.65	33	20.45	−21.9	−21.9	−22.0	20	20.44	−21.6	−21.5	−21.7
20.65−21.00	20	20.81	−22.5	−22.4	−22.6	6	20.73	−22.4	−22.3	−22.7
21.00−21.35	13	21.08	−23.0	−22.9	−23.2	3	21.07	−23.1	−22.9	−23.5
21.35−21.70	5	21.42	−23.8	−23.6	−24.1	0	...	...		

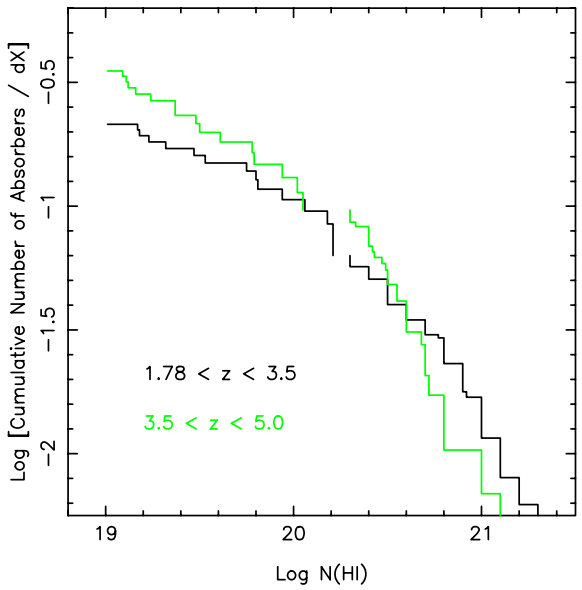

Figure 21. Cumulative number of quasar absorbers as a function of column density for two redshift intervals. The discontinuity at $\log N_{\rm H\,I} = 20.3$ illustrates that the DLA and sub-DLA samples (and associated redshift paths) are made of different quasar spectra and are therefore totally *independent*. The observations show that the incidence of low column-density absorbers is bigger at high redshift, as predicted by Péroux et al. (2003a).

density:

$$\Omega_{\rm H\,I}(z) = \frac{H_o \mu m_H}{c\rho_{\rm crit}} \frac{\sum N_i({\rm H\,I})}{\Delta X}, \quad (10)$$

where $\mu = 1.3$ is the mean molecular weight and $m_{\rm H}$ is the hydrogen mass. The total gas mass, including H I gas in systems below the canonical DLA definition, is plotted in Fig. 22 and compared with the stellar mass density today (Ω_*) and H I mass measured with radio observations of local galaxies (triangle at $z = 0$). Measurements at $z < 2$ are $\Omega_{\rm H\,I+He\,II}$ from MgII-selected DLAs (Rao et al., in preparation). The left panel of the figure decomposes the H I mass contained in both classical DLAs and in DLAs + sub-DLAs. These results are tabulated in Table 7. The right panel of the same figure shows $\Omega_{\rm H\,I+He\,II}$ derived from the homogeneous survey of DLAs found in the first data release (DR1) of the Sloan Digital Sky Survey (Prochaska & Herbert-Fort 2004).

3.4 Clustering properties

As already noted in Péroux et al. (2003b), quite a few of the 21 sub-DLAs which make up the new sample are close in redshift. The notes in the last column of Table 2 emphasize in particular those systems less than ∼400 km s^{-1} apart, which in practice means that they needed to be fitted together: $z_{\rm abs} = 3.995/3.999$ toward PSS J0133+0400 ($\Delta v = 240$ km s^{-1}), $z_{\rm abs} = 3.656/3.662$ toward BR J2215−1611 ($\Delta v = 380$ km s^{-1}) and $z_{\rm abs} = 3.690/3.696$ toward BR J2349−3712 (also have $\Delta v = 380$ km s^{-1}). Another example is the two $z_{\rm abs} = 3.692/3.773$ DLAs along PSS J0133+0400 ($\Delta v = 5100$ km s^{-1}), with (between them) a $z_{\rm abs} = 3.760$ quasar absorber just below the sub-DLA definition $\log N_{\rm H\,I} < 19.0$. In fact, the line of sight toward PSS J0133+0400 is particularly rich, containing a total of six DLAs/sub-DLAs, all except one of which are separated by no more than $\Delta v = 15000$ km s^{-1}. This complex group of systems appears to be similar to the multiple DLAs (MDLAs) studied in Lopez & Ellison (2003), which are found to have abundance patterns distinctly different from those of classical DLAs. In the present data, we do not cover the red part of the spectrum which would allow us to detect metal lines to further test the hypothesis from Lopez & Ellison (2003). Acquiring a spectrum covering the red part of this quasar would allow us to test further the hypothesis about the possibly truncated star formation of these MDLAs.

4 DISCUSSION

4.1 On the ionized fraction of sub-DLAs

The extension of the classical DLA definition to $\log N_{\rm H\,I} > 19$ proposed by Péroux et al. (2003a) has triggered concerns about the ionized fraction in these sub-DLAs. This issue is not relevant when quasar absorbers are included in the total H I gas mass of the Universe, $\Omega_{\rm H\,I+He\,II}$. Indeed, it is the sheer number of sub-DLAs which makes them add up to the classical DLA contribution, and this does not depend on the amount of gas ionized in these systems. On the contrary, the quasar absorbers which have a high ionization fraction should not be included when measuring the *neutral* gas mass, as these absorbers indicate hotter gas. Nevertheless, the evolution of neutral gas mass is most probably the result of several phenomena including star formation, galactic feedback, ionization of neutral gas and formation of molecular H_2 gas (which will in turn lead to the formation of stars). Which of these may be the dominant processes probed by DLAs and/or sub-DLAs is at present unclear.

When sub-DLAs are used for estimating global metallicity, one might rightly wonder about the fraction of the gas (and consequently metals) in ionized form. In order to address this question, Dessauges-Zavadsky et al. (2003) have carefully modelled every one of the 12 sub-DLAs making up their sample using a detailed CLOUDY model. Overall, their findings demonstrate that indeed the ionized fraction $x = H^+/H$ account for 2/3rd of the gas. However, they have also

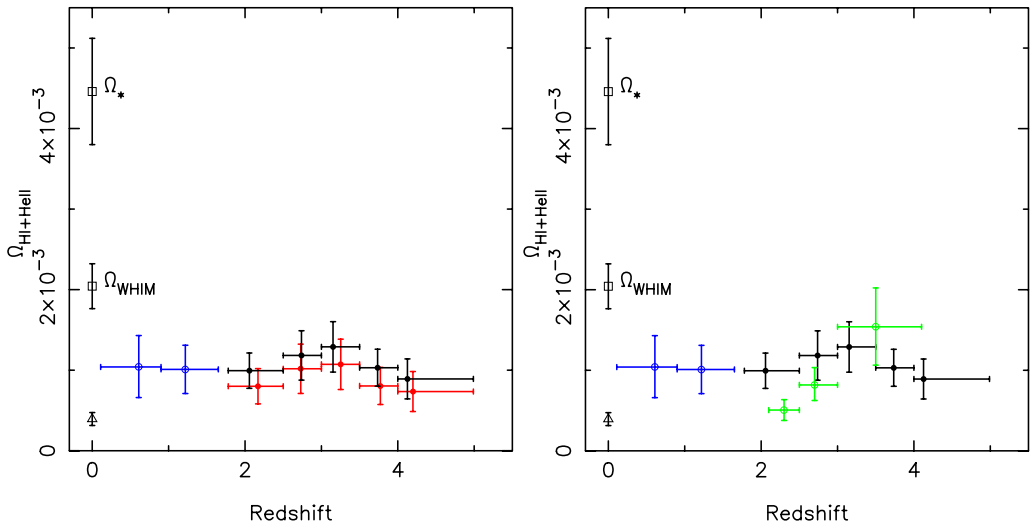

Figure 22. Redshift evolution of the gas mass density $\Omega_{\rm H\,I+He\,II}$ expressed as a fraction of the critical density. The stellar mass density today is represented by Ω_* measured by Cole et al. (2001) for a Salpeter initial mass function and the baryons in the hot gas is represented by $\Omega_{\rm WHIM}$ (WHIM being the warm-hot intergalactic medium) measured from the incidence of O VI absorbers by Danforth & Shull (2005). The triangle at $z = 0$ corresponds to the H I mass measured with radio observations in local galaxies (Zwaan et al. 2005a). The two error bars at $z < 2$ are $\Omega_{\rm H\,I+He\,II}$ from MgII-selected DLAs (Rao et al., in preparation). **Left panel:** the light grey bins at $z > 2$ are $\Omega_{\rm H\,I+He\,II}$ in systems with $\log N_{\rm H\,I} > 20.3$, while the black bins correspond to the total H I gas, including the H I contained in sub-DLAs. **Right panel:** $\Omega_{\rm H\,I+He\,II}$ derived from the first data release of the Sloan survey is shown in light grey (Prochaska & Herbert-Fort 2004) together with our measurements of the total as mass (black bins).

Table 7. Redshift evolution of the gas mass density $\Omega_{\rm H\,I+He\,II}$ contained in classical DLAs and in sub-DLAs and expressed as a fraction of today's critical density. The total amount of H I gas is given **in bold**.

$\log N_{\rm H\,I}$ range			$\log N_{\rm H\,I} > 20.3$				$19.0 < \log N_{\rm H\,I} < 20.3$						
z range	$\langle z \rangle$	dz	dX	$\Omega_{\rm DLA}$ $\times10^{-3}$	# DLA	# quasar	$\langle z \rangle$	dz	dX	$\Omega_{\rm sub-DLA}$ $\times10^{-3}$	# sub-DLA	# quasar	**Total** $\Omega_{\rm H\,I+He\,II}$
1.78−2.50	2.17	189.0	586.0	0.80±0.22	36	417	2.06	8.8	27.6	0.19±0.13	3	35	**0.99±0.22**
2.50−3.00	2.73	87.2	301.0	1.02±0.31	18	274	2.74	9.1	31.5	0.17±0.10	5	28	**1.18±0.31**
3.00−3.50	3.25	64.8	239.6	1.07±0.31	18	178	3.15	9.4	34.9	0.22±0.11	7	35	**1.32±0.31**
3.50−4.00	3.77	49.5	194.6	0.80±0.23	19	112	3.74	9.6	37.9	0.23±0.08	12	32	**1.03±0.23**
4.00−4.99	4.20	23.2	95.6	0.73±0.25	10	82	4.13	5.1	20.9	0.16±0.10	4	20	**0.89±0.25**

shown that relative or absolute abundances estimated from X^+/H^o measurements are a good approximation of, e.g., $X_{\rm tot}/{\rm Fe}_{\rm tot}$ or $X_{\rm tot}/H_{\rm tot}$. Therefore, using the metals commonly detected in sub-DLAs for a measure of the metallicity of the H I gas in the Universe *does not introduce a systematic bias*, even though the ionization fraction of the systems is not small.

4.2 On the nature of sub-DLAs

By assuming that both DLAs and sub-DLAs indicate the same underlying parent population, a natural explanation for the nature of sub-DLAs could be that they are the outermost part of galaxies (Péroux et al. 2003b). This is illustrated by the calculations of absorber sizes presented here, where the characteristic radius of sub-DLAs is around $40\,h_{100}^{-1}$ kpc and that of DLAs is $20\,h_{100}^{-1}$ kpc.

The metallicity of sub-DLAs also seems to differ from that of classical DLAs. Smoothed particle hydrodynamics simulations (Nagamine, Springel & Hernquist 2004a, b) indicate that DLAs should be 1/3 of solar metallicity at $z = 2.5$, and even more metal-rich toward lower redshifts. Indeed, there are lines of evidence pointing toward lower column-density quasar absorbers like sub-DLAs being more metal rich at $z < 2$ (Péroux et al. 2003b). This could be explained by classical DLAs being dustier than their sub-DLA counterparts. The high dust content of DLAs could act against their selection by dimming background quasars in the first place. Recent computations have shown that even current radio-selected quasar samples (Ellison et al. 2001) are not in disagreement with such a scenario (Vladilo & Péroux 2005). In fact, from figure 9a of Vladilo & Péroux (2005), it can be appreciated that in the decade $\log N_{\rm H\,I} =$ 20–21, from 10–50 per cent of the DLAs might be missed as a result of dust obscuration. Extrapolations of these mathematical formulations to the $\log N_{\rm H\,I} =$ 19–20 decade suggest that only a little under 10 per cent of the sub-DLAs might be missed by dust obscuration.

If confirmed, this can be explained by the fact that in sub-DLAs, the Zn column-density threshold does not combine with the H I threshold $\log N_{\rm H\,I} > 20.3$ that prevents the detection of sub-DLAs.

4.3 Cosmological evolution of the mass densities

Fig. 23 shows the cosmological evolution of some of the observable baryons in the Universe. In recent years, new observations have considerably changed the global picture with respect to previous studies (Lanzetta et al. 1991; Wolfe et al. 1995; Storrie-Lombardi et al.

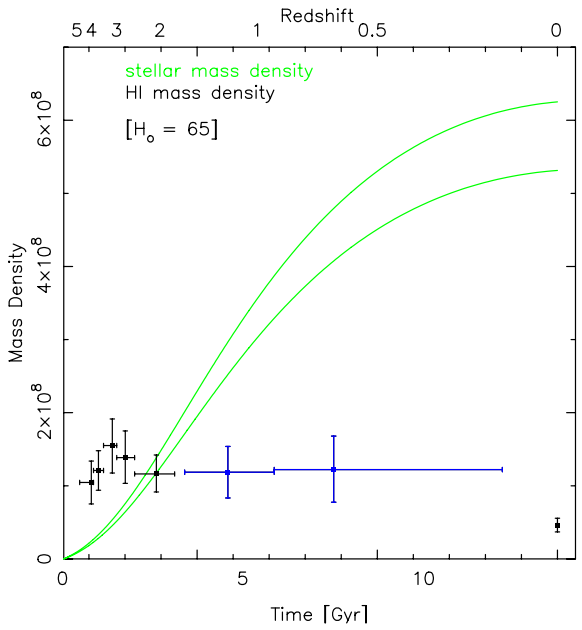

Figure 23. Observable baryons in the Universe as a function of time. The curve represents the mass density in stars from Rudnick et al. (2003) integrated from the Star Formation Rate measured by Cole et al. (2001). The uncertainties in that measurement are estimated to be around 15 per cent but are also a strong function of the chosen initial mass function. The error bars represent the mass density in those quasar absorbers deconvolved from the local critical density. A direct comparison of these two quantities illustrates the puzzling current situation concerning the baryon content of the Universe.

1996a; Storrie-Lombardi & Wolfe 2000). In Fig. 23, the direct comparison of the mass density in stars and in H I illustrates several issues:

(i) $\Omega_{\rm H\,I+He\,II}$ observed in quasar absorbers at high redshift ($z > 2$) is low compare with the mass density observed in stars today, Ω_*.

(ii) $\Omega_{\rm H\,I+He\,II}$ observed in quasar absorbers evolves little over time from $z = 5$ to $z > 0$.

(iii) $\Omega_{\rm H\,I+He\,II}$ observed in quasar absorbers at intermediate and high redshift ($z > 0$) is high compared with H I inferred from 21-cm observations of local galaxies.

(iv) $\Omega_{\rm H\,I+He\,II}$ observed in quasar absorbers over most of the age of the Universe (since the Universe was 3 Gyr old, corresponding to about $z < 2$) is not well constrained.

The first point (i) arises mostly from the fact that the most recent studies make use of modern cosmological parameters (Spergel et al. 2003), including a non-zero Λ cosmological constant, which compresses the high-redshift measurements with respect to the local ones. The possibility that large numbers of quasar absorbers are missing in optically selected quasar surveys is still hotly debated. While radio surveys looking for DLAs in quasar samples without optical limiting magnitudes (Ellison et al. 2001, 2004) show that there is not a large number of DLAs missing, other observational indicators suggest that the DLAs we know of are not extremely dusty (Pettini et al. 1997; Ledoux, Petitjean & Srianand 2003; Kulkarni et al. 2005; Murphy & Liske 2004). It should be emphasized, however, that there are two separate issues here: (a) what is the dust content of the quasar absorbers we know of today and (b) what fraction of the quasar absorbers is missed because their background quasar has not been not selected in the first place? An extension of Fall & Pei (1993) calculations, taking into account the most recent observations, addresses both these issues: Vladilo & Péroux (2005) show that whilst the dust content of the DLAs in the current sample is not too high, the missing fraction is possibly quite important, ranging from 30–50 per cent at $z = 1.8$–3.0.

Concerning points (ii) and (iii), the number of quasar absorbers observed at $z > 2$ is now reaching the hundreds. The mild fluctuations in the redshift evolution in the range $z = 5$ to $z = 2$ is within the small error estimates. Therefore the cosmological evolution of the total gas mass, $\Omega_{\rm H\,I+He\,II}$, can be approximated to constant in that redshift range. Yet, radio observations of very large numbers of local H I-rich galaxies such as the H I Parkes All-Sky Survey (Zwaan et al. 2005a) indicate a low value of $\Omega_{\rm H\,I+He\,II}$ at $z = 0$. This would imply a fast evolution of the gas mass between $z \sim 0.61$ (Rao et al., in preparation) and $z = 0$.

The last point illustrates how challenging it still is to find and study quasar absorbers at intermediate redshifts. Warnings about $\Omega_{\rm H\,I+He\,II}$ measurements based on small number statistics have already been issued (Péroux et al. 2004b) and unfortunately future developments in that direction appear limited given the presently restricted availability of UV optimized instruments.

5 CONCLUSION

We have presented a new sample of high-redshift sub-DLAs ($N_{\rm H\,I} > 10^{19}\,{\rm cm}^{-2}$) found in the spectra of 17 $z > 4$ quasar spectra observed with the Ultraviolet-Visual Echelle Spectrograph on VLT. The statistical properties of this sample of 21 new sub-DLAs is analysed in combination with another 10 sub-DLAs from previous ESO archive studies. This homogeneous sample allows us to determine the redshift evolution of the number density of DLAs and sub-DLAs and compare it with that of LLSs taken from the literature. All these systems seem to be evolving in the redshift range from $z = 5$ to $z \sim 3$. Assuming that all the classes of absorbers arise from the same parent population, estimates of the characteristic radii are provided. R_* increases with decreasing column density, and decreases with cosmological time for all systems. The redshift evolution of the column-density distribution, f(N,z), down to $N_{\rm H\,I} = 10^{19}\,{\rm cm}^{-2}$ is also presented. A departure from the usually fitted power law is observed in the sub-DLA regime. f(N,z) is further used to determine the total H I gas mass in the Universe at $z > 2$. The complete sample shows that sub-DLAs are important at all redshifts from $z = 5$ to $z = 2$ and that their contribution to the total gas mass $\Omega_{\rm H\,I+He\,II}$ is $\sim$20 per cent or more if compared with the Sloan results (Prochaska & Herbert-Fort 2004). Finally, we discuss the possibility that sub-DLAs are less affected by the effects of dust obscuration than classical DLAs.

ACKNOWLEDGMENTS

We would like to thank Nicolas Bouché for letting us publish here for the first time portions of the UVES red spectrum of SDSS J0124+0044. We are grateful to Sandhya Rao for communicating results in advance of publication. CP thanks Martin Zwaan for shared enthusiasm on the topic and the Institute of Astronomy in Cambridge for a visit during which part of this work was completed. This work was supported in part by the European Community Research and Training Network 'The Physics of the Intergalactic Medium'.

REFERENCES

Blanton M. R. et al., 2003, ApJ, 592, 819
Boissier S., Péroux C., Pettini M., 2003, MNRAS, 338, 131
Bouché N., Lowenthal J. D., 2004, ApJ, 609, 513

Cole S. et al., 2001, MNRAS, 326, 255
Chen H.-W. et al., 2003, ApJ, 586, 745
Danforth C. W., Shull J. M., 2005, ApJ, 624, 555
Dessauges-Zavadsky M., Péroux C., Kim T. S., D'Odorico S., McMahon R. G., 2003, MNRAS, 345, 447
Ellison S. L., Lopez S., 2001, A&A, 380, 117
Ellison S. L., Yan L., Hook I. M., Pettini M., Wall J. V., Shaver P., 2001, A&A, 379, 393
Ellison S. L., Churchill C. W., Rix S. A., Pettini M., 2004, ApJ, 615, 118
Fall S. M., Pei Y. C., 1993, ApJ, 402, 479
Fontana A., Ballester P., 1995, The Messenger, 80, 37
Holmberg E., 1975, in Prantzos N., Tosi M., Von Steiger R., eds, Galaxies and the Universe. Kluwer, Dordrecht, p. 127
Khare P., Kulkarni V. P., Lauroesch J. T., York D. G., Crotts A. P. S., Nakamura O., 2004, ApJ, 616, 86
Kulkarni V. P., Fall S. M., 2002, ApJ, 580, 732
Kulkarni V. P., Fall S. M., Lauroesch J. T., York D. G., Welty D. E., Khare P., Truran J. W., 2005, ApJ, 618, 68
Lanzetta K., McMahon R.G., Wolfe A., Turnshek D., Hazard C., Lu L., 1991, ApJS, 77, 1
Ledoux C., Petitjean P., Srianand R., 2003, MNRAS, 346, 209
Levshakov S. A., D'Odorico S., Agafonova I. I., Dessauges-Zavadsky M., 2004, A&A, 413, L827
Lopez S., Ellison S. L., 2003, A&A, 403, L573
Lopez S., Maza J., Masegosa J., Marquez I., 2001, A&A, 366, 387
Malaney R. A., Chaboyer B., 1996, ApJ, 462, 57
Murphy M. T., Liske J., 2004, MNRAS, 354, L31
Nagamine K., Springel V., Hernquist L., 2004a, MNRAS, 348, 421
Nagamine K., Springel V., Hernquist L., 2004b, MNRAS, 348, 435
Pei Y. C., Fall S. M., 1995, ApJ, 454, 69
Pei Y. C., Fall S. M., Hauser M. G., 1999, ApJ, 522, 604
Péroux C., Storrie-Lombardi L., McMahon R., Irwin M., Hook I., 2001, AJ, 121, 1799
Péroux C., McMahon R., Storrie-Lombardi L., Irwin M., 2003a, MNRAS, 346, 1103
Péroux C., Dessauges-Zavadsky M., D'Odorico S., Kim T. S., McMahon R., 2003b, MNRAS, 345, 480
Péroux C., Petitjean P., Aracil B., Irwin M., McMahon R. G., 2004a, A&A, 417, 443
Péroux C., Deharveng J.-M., Le Brun V., Cristiani S., 2004b, MNRAS, 352, 129
Peterson B. M., Strom S. E., Strom K. M., 1979, AJ, 84, 735
Pettini M., Smith L. J., King D. L., Hunstead R. W., 1997, ApJ, 486, 665
Prochaska J. X., Herbert-Fort S., 2004, PASP, 116, 622
Prochaska J. X., Gawiser E., Wolfe A. M., Cooke J., Gelino D., 2003, ApJS, 147, 227
Rudnick G. et al., 2003, ApJ, 599, 847
Schechter L., 1976, ApJ, 203, 297
Schneider D. P. et al., 2002, AJ, 123, 567
Spergel D. N. et al., 2003, ApJS, 148, 175
Steidel C., Kollmeier J. A., Shapley A. E., Churchill C. W., Dickinson M., Pettini M., 2002, ApJ, 570, 526
Steidel C., Adelberger K. L., Shapley A. E., Pettini M., Dickinson M., Giavalisco M., 2003, ApJ, 592, 728
Storrie-Lombardi L., Wolfe A., 2000, ApJ, 543, 552
Storrie-Lombardi L., McMahon R., Irwin M., 1996b, MNRAS, 283, L79
Storrie-Lombardi L., Irwin M., McMahon R., 1996a, MNRAS, 282, 1330
Storrie-Lombardi L., Irwin M. J., McMahon R. G., Hook I. M., 2001, MNRAS, 322, 933
Stern D., Spinrad H., Eisenhardt P., Bunker A. J., Dawson S., Stanford S. A., Elston R., 2000, ApJ, 533, L75
Tytler D., 1981, Nat, 291, 289
Vladilo G., Péroux C., 2005, A&A, submitted
Wolfe A., Lanzetta K. M., Foltz C. B., Chaffee F. H., 1995, ApJ, 454, 698
Zwaan M. A. et al., 2003, AJ, 125, 2842
Zwaan M. A., Meyer M. J., Staveley-Smith L., Webster R. L., 2005a, MNRAS, 359, L30
Zwaan M. A., van der Hulst J. M., Briggs F. H., Verheijen M. A. W., Ryan-Weber E. V. 2005b, MNRAS, submitted

This paper has been typeset from a TEX/LATEX file prepared by the author.